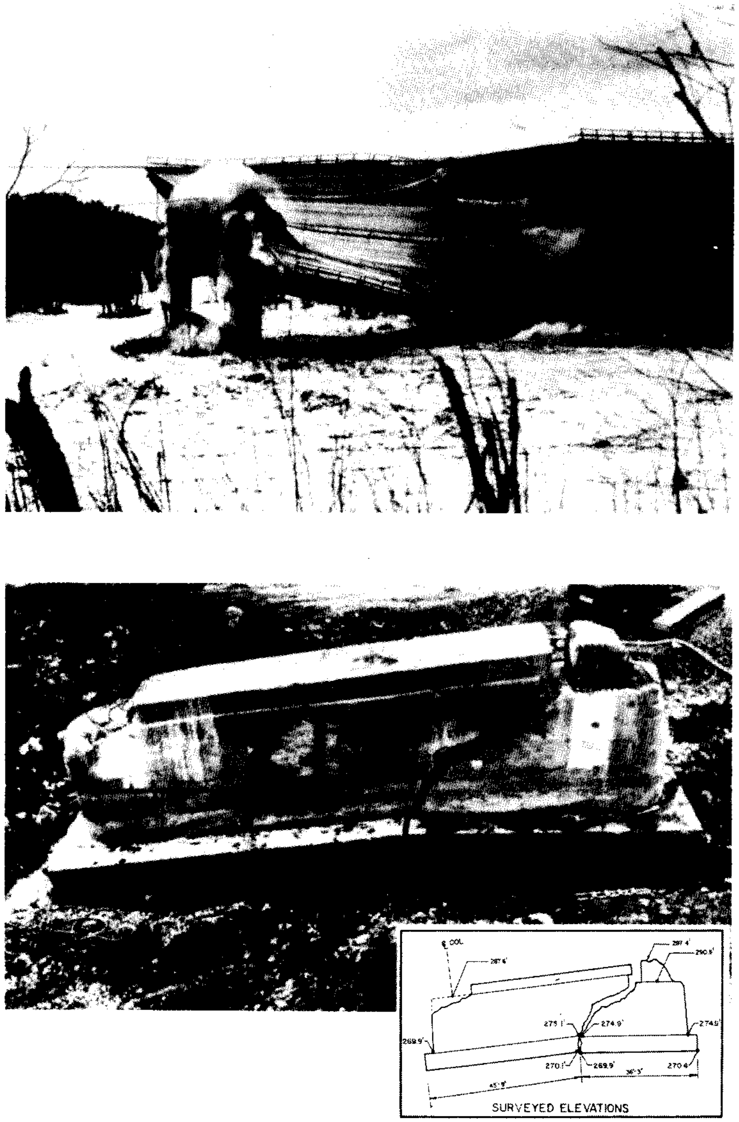

Fig. 4--(a) Size effect for structural strength as predicted by linear or nonlinear fracture mechanics, (b) estimated size effect for the strength of the concrete plinth (Reference 34)

Fracture Resistance of Acrylic Fiber Reinforced Mortar in Shear and Flexure

by R.J. Ward, K. Yamanobe, V.C. Li, and S. Backer

Synopsis: The results of notched beam, direct tension, splitting tension, compression, shear beam and flexural tests on plain mortar and on mortar reinforced with different volume fractions of short acrylic fibers are reported. An indirect J-integral technique is employed to determine the tension-softening curve and thus the tensile strength, the fracture energy and the critical crack opening from the notched beam test results. As the volume fraction of fibers is increased the strength in shear and flexure, the fracture energy and the critical crack opening all increase, the tensile strength remains essentially constant and the compressive strength shows some reduction. The characteristic length l_{ch} is used as a material property to characterize the post peak tensile behavior. The shear and flexural strengths are related to the normalized dimension d/l_{ch} and good agreement between the experimental results and theoretical predictions of decreasing strength with increasing d/l_{ch} is found.

Keywords: acrylic resins; fiber reinforced concretes; flexural strength; fracture properties; mortars (material); shear strength; synthetic fibers; tensile strength

Robert J. Ward is a research assistant in the Department of Civil Engineering at the Massachusetts Institute of Technology, Cambridge, MA 02139, USA.

Koji Yamanobe is a visiting research engineer in the Department of Civil Engineering at the Massachusetts Institute of Technology from the Shimizu Institute of Technology, Tokyo, Japan.

Victor C. Li is an Associate Professor of Civil Engineering at the Massachusetts Institue of Technology, Cambridge, MA 02139, USA.

Stanley Backer is a Professor of Mechanical Engineering at the Massachusetts Institute of Technology, Cambridge, MA 02139, USA.

INTRODUCTION

A major deficiency in concrete as a structural material is its brittle behavior. An effective means of improving the fracture toughness of concrete is to reinforce it with fibers. Recent research in synthetic fiber reinforced concrete (FRC) suggests that significant improvement in toughness could be achieved with just a few percentage volume fraction of nylon, acrylic and other fibers [1,2], even though the tensile strength of the composite appears to remain essentially constant. Apart from obvious increase in resistance against fracture extension, the synthetic FRC represents a material with a larger material characteristic length l_{ch}, defined by $l_{ch}=J_cE/f_t^2$ where J_c is the fracture energy, E is the modulus of elasticity and f_t is the tensile strength. J_c is defined as the amount of energy necessary to create a unit area crack and is equal to the area under the tension softening curve.

The significance of the material characteristic length, l_{ch}, in determining structural behavior has been discussed in several papers. Li and Liang [3] expressed the propensity of a transition from brittle fracture failure for a material with small l_{ch} to tensile 'yield' failure for a material with large l_{ch} in a given structure. Recent experimental work [4] and theoretical work [5, 6, 7, 8] both show that concrete beams, subjected to flexural and shear loading, fail with decreasing loads with respect to the normalized dimension d/l_{ch}. For a given material (fixed l_{ch}), then, this implies that structures with larger size decrease in load bearing capacity. This is known generally as the size effect. For a given structural dimension d, the change of material property reflected in l_{ch} will then also have an effect on the structural load bearing capacity. This paper presents preliminary experimental results which quantify this effect.

Apart from the effect of l_{ch} on the structural behavior,the shape of the tension-softening curve has also been shown to be important in influencing structural behavior [3]. This effect is also briefly studied.

In this paper, the change in l_{ch} is effected by using different volume fractions of acrylic fibers ranging from 0 to 3%, in a mortar mix. Both material and structural tests were carried out. The main material property tests include compression tests, direct and splitting tensile tests, and fracture energy tests. The structural tests include tests of beams subject to flexure and shear loads.

The test results suggest that small volume fractions of low modulus fibers do not significantly affect the pre-peak stress strain curve in tension, but do have a major influence on the tension-softening curve giving rise to increases in the fracture energy and the characteristic length of the order of 500%. This phenomenon may lead to significant increases in the ultimate load bearing capacity of structures in which a fracture zone starts to develop prior to peak load. Results presented in this paper for beams tested under shear and flexure support this idea. Some reduction in the compressive strength of cylinders was observed, as the volume fraction of fibers increased, due to incomplete compaction. It is believed that this problem can be overcome by better compaction techniques and greater use of plasticizer. Flexural tests on two different beam types suggest that the beneficial effects of fibers may be much greater in specimens where significant initial shrinkage stresses exist.

In the following sections, we first describe details of the test program and the preparation of specimens. The test procedures and results will then be presented, followed by a discussion on the implication of the test results.

RESEARCH PROGRAM

The primary objective of this program was to investigate the influence of the tension-softening, σ–δ, curve on the behavior of concrete under various loading configurations which give rise to tensile stresses. In order to achieve significant variations in the σ–δ curve without much change in the pre-peak stress-strain, σ–ε, curve it was decided to reinforce plain mortar with different volume fractions of low modulus and relatively low strength acrylic fibers. Four volume fractions, 0, 1, 2 and 3% were used to produce four different σ–δ curves.

The experimental program involved the following tests:

(a) Notched beam test: 32 notched beams with dimensions 63.5 x 114.3 x 432 mm were tested to indirectly obtain tension softening curves and also to calculate values for G_F defined using the area under the load-deflection curve of a notched beam.

(b) Direct tension test: 46 specimens (22 with dimensions 40 x 50 x 100 mm and 24 with dimensions 50 x 60 x 110 mm) were tested in direct tension to examine the ultimate strengths and also the effect of non-uniform straining on the apparent tensile strength.

(c) Splitting tension test: 45 specimens with dimensions 50 x 55 x 65 mm were tested to calculate the splitting tensile strengths.

(d) Compression test: 37 cylindrical specimens (diameter = 77 mm, height = 150 mm) were tested to obtain the compressive strength and also the modulus of elasticity. The importance of compaction when using fiber reinforced concrete was also examined.

(e) Shear beam test: 12 beams, reinforced longitudinally with two #3 rebars corresponding to 2% of cross sectional area, were tested to calculate the shear strengths. Beam dimensions were similar to the notched beams and the span-depth ratio when loaded was 2.0.

(f) Flexural Test: 24 beams were tested under four-point bending to obtain the flexural strengths. 10 of the beams had dimensions similar to the notched beams and the other 14 were 51 mm deep, 63.5 mm wide and spanned 153 mm. These tests provided information regarding the influence of beam depth and characteristic length on flexural strength.

SPECIMEN PREPARATION

The following materials were used.

(1) Type III rapid hardening portland cement.
(2) Sand, passed through a #8 sieve (size = 2.36 mm).
(3) Acrylic fibers with the following properties:
    length = 6.35 mm
    diameter = 13.6 μm
    density = 1.15 g/cc
    tensile strength = 300 MPa
    initial modulus of elasticity = 5.5 GPa
(4) #3 rebars, grade 40
    yield stress = 440 MPa
    tensile strength = 670 MPa.

The cement : sand : water ratio was 1 : 1 : 0.5. For volume fractions of 2 and 3% 17.5 cc of superplasticizer per 1 kg of cement was added with the water to improve workability. The plasticizer used was a high range water reducing admixture named Daracem-100 and is classified as ASTM C-494 Type A.

A new Omni-mixer in which random movement of particles is induced to occur by a wobbling flexible drum bottom was used. The absence of agitating blades ensured more uniform fiber distribution. Initially the sand, cement and fibers were mixed dry for 3 minutes. Then the water and plasticizer (when appropriate) were added and mixed for a further 3 minutes. Fiber distribution appeared to be much better than if the water had been added initially.

Compaction was achieved using a vibrating table and a tamping rod. The specimens were covered in plastic for 15 hours after casting and were then removed from the molds and placed in water at 22°C until 7 days old. They were then removed and allowed to dry at room temperature until testing. Most tests were carried out at 14 days with some at 40 and 60 days. For the notched beams the notches were cast using 0.8 mm thick aluminum plates which were removed after 15 hours. Mold release facilitated easy removal.

TESTING PROCEDURE AND RESULTS

Notched Beam Test

The stress-deformation behavior of concrete in tension can be described fully by means of two relationships [6]. The first is the conventional stress-strain curve. The second is a stress-deformation, σ–δ, relationship, known as the tension-softening curve which defines a functional relationship between the traction acting across a crack plane and the separation distance of the crack faces. The total energy absorbed during deformation can be described fully by these two curves as shown in Fig. 1.

The area enclosed by the σ–ε curve between loading and unloading branches corresponds to inelastic energy absorption, presumably due primarily to distributed microcracking at the cement aggregate interface prior to peak stress, per unit volume of material. The area under the σ–δ curve corresponds to energy absorbed within the fracture process zone when a unit area traction free crack is formed. Both curves can be obtained from a stable direct tension test. However, an inherent difficulty with this test is the stability of loading the specimen during the softening process and in many cases existing loading machines must be stiffened and feedback control loading systems used in order to obtain the σ–δ relationship [6,9]. These modifications are too complicated to allow the measurement of the σ–δ curve to become standard practice in normal testing laboratories. In this research program an indirect J-integral technique, proposed by Li [10], has been used to calculate tension-softening curves. The advantages of this method are as follows:

(a) Simple testing procedure
(b) Simple testing machine
(c) Small specimens.

Summary of J-integral technique--A full description of this technique can be found in [11,12]. The J-integral [13] evaluated along a contour Γ surrounding the elongated process zone near the macrocrack tip as in Fig. 2 can be expressed as:

$$J(\delta) = \int_0^{\delta} \sigma(\delta)\, d\delta \tag{1}$$

where δ is the separation at the physical crack tip and $\sigma(\delta)$ is the corresponding stress-transferring capability across the process zone. J can be obtained experimentally from a compliance test by loading two precracked specimens with slightly different crack lengths. If the load P, the load point displacement Δ, and the crack tip separation δ, are measured simultaneously in the test then J can be obtained in terms of Δ from the area $A(\Delta)$ between the two P-Δ curves up to a load point displacement of Δ as:

$$J(\Delta) = \frac{A(\Delta)}{B(a_2 - a_1)} \tag{2}$$

where B is the specimen width and $(a_2 - a_1)$ is the difference in the initial crack lengths of the two specimens. $J(\Delta)$ can then be converted to $J(\delta)$ using a Δ–δ relationship. Differentiation of Eq. (1) leads to

$$\sigma(\delta) = \frac{\partial J(\delta)}{\partial \delta} \tag{3}$$

which is the tension-softening relationship of the material. The critical J-integral value, J_c, is defined as:

$$J_c = \int_0^{\delta_c} \sigma(\delta)\, d\delta \tag{4}$$

where δ_c is the value of the critical crack separation at the end of the tension-softening curve when σ=0 and J_c is equal to the total area under the tension-softening curve.

The above technique was employed in a four point beam bending configuration as outlined in Fig. 3. For each fiber volume fraction a total of 8 beams were tested; 4 with an initial notch length of 42 mm and 4 with notch length 50.5 mm. A displacement-controlled loading machine was used. The fiber reinforced concrete specimens were loaded at an initial rate of 0.0254 mm/min; this being changed to 0.0508 mm/min when the load dropped to 30% of the peak value and later to 0.127 mm/min to ensure a reasonable test time. The time to maximum load varied from 15 minutes for $V_f = 1\%$ to about 22 minutes for $V_f = 3\%$ with the total testing time varying between 40 and 55 minutes. The plain mortar specimens were loaded at a rate of 0.0127 mm/min with maximum load reached after about 18 minutes and complete failure after about 40 minutes. All tests were continued until the beams failed under self-weight.

The average vertical displacement of the two loading points was measured using a linear variable displacement transducer (LVDT). A second LVDT, placed in a horizontal position at the notch tip, was used to measure the crack tip opening displacement. The LVDT and its target were placed 14 mm apart on opposite sides of the notch tip.

Results--Appendix A contains load versus load point displacement and load point displacement versus crack tip separation curves for all the beam tests. Due to the relatively large scatter in the results for $V_f = 0\%$ (Fig. A-1) a separate set of tests on plain mortar beams was carried out using notch lengths of 58 and 65 mm. The corresponding load-deflection curves are shown in Fig. A-5. These results were used to calculate the tension-softening curve for $V_f = 0\%$. Fig. 4 shows the deduced tension-softening curves for each volume fraction. Using the load versus load point displacement curves it was possible to calculate G_F [14] and f_f(net) for each test where G_F and f_f(net) are defined as:

$$G_F = \frac{A}{B(d-a)} \tag{5}$$

$$f_f(\text{net}) = \frac{6M_{max}}{B(d-a)^2} \tag{6}$$

and A is equal to the total area under the curve including a correction for self-weight recommended by Petersson [6], B is the specimen width, d is the depth, a is the notch length and M_{max} is the maximum bending moment at the notched section. G_F can be used as an approximate measure of fracture energy but has been shown to be dependent on the beam size used to determine it [15]. Table 1 shows the calculated G_F (corrected for self-weight) and f_f(net) values for each test and also the magnitude of the self-weight correction applied to G_F. Each beam name has a number corresponding to the fiber volume fraction and a letter corresponding to the initial notch length where A, B, C and D represent a 42 mm notch and E, F, G and H a 50.5 mm notch. The G_F values for beams 1G, 2C and 3F were not considered valid due to exceptional deviations from the average values. Some instability after peak load was noted in tests OE and OF. All other tests were stable at all times during the test.

Table 2 gives details of the results obtained from the indirect J-integral method and also average G_F values for each volume fraction. The deduced tensile strength, f_{td}, is obtained from $[\sigma(\delta)]_{max}$ where $\sigma(\delta)$ is defined in Eq.(3).

The deduced tensile strength does not vary significantly with volume fraction. This result is expected for these volume fractions of a low modulus fiber as will be explained in greater detail later. The δ_c value is increased significantly with fibers but does not differ greatly for different fiber volume fractions in the 1 to 3% range. The δ_c values are less than half the fiber length due to the fact that these fibers form a relatively strong bond with the matrix and tend to rupture rather than pull out along the fractured surface. The correction which should be applied to the G_F values to account for self-weight is larger (percentagewise) for low fracture energy material.

Fig. 5 shows J_c and G_F values for each volume fraction. There is a significant increase in the energy absorption ability as the fiber volume fraction is increased. The increase is approximately 700% when 3% volume fraction is used. This is achieved by fiber breakage and pull-out after the matrix has cracked. Also from Fig. 5 it can be seen that the difference between J_c and G_F increases as volume fraction is increased. This can be explained by examining energy losses outside the fracture zone. It is probable that prior to localization of deformation onto the cracking zone that diffuse inelastic deformation is occurring in the material adjacent to the zone, and thus there is an energy loss. Some loss also occurs due to localized crushing at the support points. Since the maximum load increases significantly with volume fraction (Figs. A1-A4) it is expected that energy losses outside the fracture zone also increase. This leads to increasing overestimation by G_F of actual energy absorption in the fracture plane as volume fraction increases. In the J-integral method the difference between two beams under similar states of stress is obtained and thus energy losses outside the fracture zone tend to cancel out. It is also believed that J_c is independent of the beam size used to calculate it. The effect of self-weight is significant for the G_F calculation but does not need to be accounted for when calculating J_c. These are some advantages of the indirect J-integral method. However, for plain concrete ($V_f = 0\%$) the simple G_F test appears to give quite accurate results for fracture energy, at least for the specimen size used for the present series of experiments.

Tension Tests

Direct tension test--Two specimen types, A and B, were used in this test. Type A had dimensions 40 x 50 x 100 mm, were cast in individual molds, and were tested after 14 to 17 days. Type B had dimensions 50 x 60 x 110 mm, were cut from the ends of the notched beam specimens after the fracture test and were tested at an age of 40 - 45 days. The ends of each specimen were ground to remove loose cement and ensure that they were parallel. 77 mm diameter steel plates were glued to each end using 5-minute epoxy. The specimens were tested as shown in Fig. 6 with no restriction on rotation. Figs.7a and 7b show the average tensile stress, f_t, across each specimen at failure for each volume fraction. These test results show quite a large scatter and also an apparent increase in the tensile strength as the volume fraction is increased. An approximate argument is now presented which explains why tensile strength is not expected to show significant change due to fibers and also why these tests show an apparent strength increase. The following notation is used:

σ_m = failure stress of matrix in tension
σ_f = failure stress of fiber in tension
E_m = modulus of elasticity of matrix
E_f = modulus of elasticity of fiber.

For this argument assume $\sigma_m = 2.6$ MPa, $\sigma_f = 300$ MPa, $E_m = 20$ GPa, $E_f = 5.5$ GPa. The fibers are arranged in a random three-dimensional pattern. A typical efficiency factor to account for fiber orientation would be 0.2 [16]. The bond strength between acrylic fibers and cement matrix is high relative to the fiber strength [1] and thus stress equal to the tensile strength can be developed in the fiber throughout the greater part of its length except for a short distance at each end. The critical length, defined as the maximum length of a single fiber which can be pulled out of a matrix without rupture, was measured by Wang et al [1] for 19.2 μm diameter acrylic fibers in cement paste and was found to be of the order of 1 mm. An efficiency factor should be used to account for the fact that in practice the fibers are not continuous and separated but rather are short and in different sized bundles. This calculation does not account for this and so gives an upper bound for the composite tensile strength. Assuming a linear stress-strain curve for the matrix, the strain at failure is 0.00013. The corresponding stress in the fibers is 0.715 MPa which is negligible. After matrix cracking the maximum load which could be transferred across the crack by fibers alone is given as 0.2 x 0.03 x 300 = 1.8 MPa for a volume fraction of 3%. This would not lead to a tensile strength increase.

The apparent strength increase with fibers can be explained using the "weakest link in the chain" idea. Suppose a critical flaw exists in a mortar specimen on one side of the center line. As the load is applied to the specimen the flawed material deforms more than other material and leads to a rotation of the specimen which is allowed by the loading configuration. Eventually the material in the flaw reaches its ultimate strength (much less than the average over all the specimen) and starts to soften as a fracture zone initiates on one side of the specimen. This leads to even more rotation. Crack propagation through the section results in sudden failure at an average stress which is much less than the

average strength of the material. This phenomenon has been confirmed by measuring displacements on opposite sides of some tension specimens using two LVDTs. Fig. 8 shows typical stress-strain relationships for each specimen side.

When the material is fiber-reinforced, significant stresses can be transferred across the softening zone which resist rotation of the specimen and lead to an increase in the average stress at failure. The direct tensile tests always give a lower bound for the average strength of the weakest section when rotation is allowed. As the fiber volume fraction is increased, this lower bound approaches the actual average strength value.

Table 3 gives the average values of the apparent tensile strength f_t for each volume fraction at two different ages. Using the above argument it can be deduced that

f_t (14-17 days) ≥ 2.6 MPa
f_t (40-45 days) ≥ 2.9 MPa.

A comparison may be made with the results from the indirect J-integral test which produced a tensile strength of approximately 2.1 MPa for each volume fraction. This value is 20% lower than the expected value of 2.6 MPa or greater. One reason for this may be loading rate. For the indirect J-integral test the maximum load was reached after about 20 minutes compared to about 10 minutes for the direct tension test. Another more important reason is that the difference in notch lengths is a finite value and does not approach zero as required by the theoretical analysis. Presently the idea of using various notch length differences and extrapolating to $\Delta a \rightarrow 0$ is being examined and it is believed that this technique will produce a tension-softening curve with a deduced tensile strength which is much closer to the actual strength. The deduced value is taken as a lower bound which approaches the true value as $\Delta a \rightarrow 0$.

Splitting tension test--The specimens used in this test were cut from the ends of the beams used in the fracture test. Specimen size was 50 x 60 x 65 mm and the testing age was 60 days. The line loading was applied along the 60 mm side via hexagonal steel bars with a 2 mm contact width. The loading rate was 0.254 mm/min and time to failure about 4 minutes. The tensile strength f_{st} was calculated as $(2P/\pi A)$ where P is the maximum load and A is the area of the split section, equal to 3000 mm^2. Fig.9 shows the test results and Table 3 gives the average values for each volume fraction.

In this test strains were approximately equal throughout the critical section and so little variation in observed tensile strength with volume fraction was expected. This is confirmed by the tests. Also the f_{st} values of approximately 3.7 MPa agree with the direct tension test which predicted $f_t \geq 2.9$ MPa at 40-45 days.

Compression Test

37 compression cylinders (diameter = 77 mm, height = 150 mm) were tested. The age at testing was 14 days for 12 specimens and 28 days for the remainder. The results for different ages did not differ significantly, and are presented together. The modulus of elasticity was measured using average displacement readings taken from two LVDTs placed on opposite sides of each cylinder with 100 mm spacing between holder and target. The crosshead speed was 1.2 mm/min and failure occurred after about 2 minutes.

In order to estimate the importance of compaction when using synthetic fiber reinforced concrete, 6 cylinders with volume fractions of 2 or 3% were compacted more thoroughly than usual. For these cylinders and for 5 normally compacted specimens of the same volume fractions the void ratio, e, relative to a plain mortar specimen was calculated as follows:

$$e = (1 - V_f)\left(1 - \frac{\rho_s - V_f \rho_f}{(1 - V_f)\rho_m}\right) \qquad (7)$$

ρ_m = density of plain mortar specimen

ρ_f = fiber density

V_f = fiber volume fraction

ρ_s = specimen density

Figs. 10 and 11 show measured compressive strengths and moduli of elasticity for each volume fraction. Table 4 gives average values for f_c and E. Table 5 shows the effect of relative void ratio on compressive strength. Results for 2C and 3C refer to the specimens in which greater compaction was achieved through more frequent use of the tamping rod. For V_f equal to 2% the average void ratio was reduced from 5.75% to 3.26% and the strength increased from 37.8 MPa to 48.3 MPa through increased compaction. For V_f equal to 3% the void ratio dropped from 7.88% to 3.6% and strength increased from 34.0 MPa to 48.0 MPa. Relatively large voids were noted in the outer part of the cylinders and were a direct result of inadequate compaction close to the mold wall. The effect of these voids was compounded by the small specimen size. In large practically sized applications this effect would be much smaller and by using adequate plasticizer it is believed that the drop off in compressive strength would be minimal. However caution is necessary for applications where compaction may be difficult such as in heavily reinforced beam sections.

Shear Beam Test

12 shear beams (3 for each volume fraction) with dimensions 63.5 x 114.3 x 432 mm were tested under three point bending as shown in Fig. 12. The span depth ratio was 2.0. Each beam contained two #3 rebars corresponding to 2% of the total cross sectional area. A displacement controlled loading machine with capacity 890 kN was used. The midspan load was measured with a pressure gage connected to the machine and the load point displacement with an LVDT. The initial cross head speed was 0.6 mm/min and was increased to 1.8 mm/min after maximum load. The peak load was reached after about 5 minutes. The tests were continued up to a load point displacement of 4 mm except for two plain mortar beams which were displaced through 1.5 mm. Two beams for each volume fraction were loaded monotonically and the third was loaded cyclically.

Appendix B contains shear stress versus load point displacement curves for each test. The shear stress is defined as the shear force divided by the total cross sectional area. The crack propagation pattern was similar for each beam type and the development for a typical beam is illustrated in Fig. 13. A visible shear crack initiated halfway between the load and support points and started to propagate diagonally towards each point. Maximum load was reached as the crack approached these points and further crack opening resulted in a decrease in the load. Fig. 14 and Table 6 show the shear strength, f_v, the displacement at maximum load, δ_v, and the shear stress when the first visible crack appears, f_{vc}, as functions of volume fraction.

Shear strength shows a modest increase of 12% between volume fractions of 0 and 3%. The stress at first cracking, however, shows a significant increase of 50%. Shear resistance is provided by dowel action of the rebars, shear friction between the crack faces and tensile stresses transferred across the cracking zone. The first two components of this resistance are not expected to change with volume fraction but the third changes according to the tension softening curve. In the next section some theoretical work [7] relating the tension softening curve to the ultimate shear strength is examined and the predictions are compared to these experimental results.

Flexural Test

Two specimen types were used in this test. The first type had dimensions 63.5 x 114.3 x 432 mm and was loaded under four-point bending with a span of 381 mm as shown in Fig. 3. 10 beams of this type were cast, 4 for 0%, 3 for 2% and 3 for 3% volume fraction. The age at testing was 14 days. The loading rate was 0.0508 mm/min and time to maximum load varied from 12 to 20 minutes. The second specimen type was cut from the ends of the notched beam specimens, had dimensions 63.5 x 51 x 216 mm and was loaded under four-point bending with a span of 153 mm as shown in Fig. 15. The age at testing was 60-65 days. The loading rate was 0.254 mm/min and time to maximum load was about 2.5 minutes.

Fig. 16 shows flexural strength, f_f, as a function of volume fraction. Table 7 gives average flexural strength for each beam type. The flexural strength, f_f, is defined as $6M/Bd^2$ where M is the bending moment over the central part of the beam when failure occurs and B and d are beam width and depth respectively.

Fig. 16 shows a significant increase in f_f as fiber volume fraction is increased and also when beam depth is decreased. These results also suggest that the fiber effect is much more pronounced for the larger beams. The effect of volume fraction on flexural strength can be explained in terms of the tension softening curve and this will be examined in detail in the next section of this paper. There are a number of reasons why the small beams show a higher strength than the larger ones. The loading rate and the testing age may account for an increase of the order of 20% [17]. Beam depth and initial shrinkage stresses also affect the flexural strength and these will be discussed in detail in the next section.

APPLICATIONS OF FRACTURE MECHANICS

Traditional strength theory which uses the stress-strain curve in tension to predict the ultimate load carrying capacity of structures which fail due to tensile stresses has been found to be inadequate when applied to a non-yielding material such as concrete which shows softening behavior throughout a localized fracture zone after the peak stress has been reached. An example of the limitations of this theory is its inability to predict the depth dependence of the ultimate strength of unreinforced concrete beams subjected to bending stresses or reinforced beams subjected to shear stresses. The fracture mechanics approach considers the complete material behavior during tensile fracture as described in Fig. 1 by both the stress-strain curve up to the tensile strength and the tension-softening curve which models the behavior of the material in the fracture zone as the crack width increases. A major objective of this research program was to examine the validity of this latter approach and this was achieved experimentally by performing shear and flexure tests on four different concrete qualities which had similar stress-strain curves but significantly different tension-softening curves. Whereas conventional strength ideas predict similar strengths for all four qualities, fracture mechanics takes account of the changing $\sigma-\delta$ curve in order to predict a strength function. In this discussion a comparison of experimental results with the fracture mechanics approach based on the "fictitious crack model" [18,19,20,6,7] will be given for both the shear and flexural tests.

The complete material behavior is characterized by the two curves in Fig. 1. An important relationship between the slopes of these two curves is defined by the material characteristic length l_{ch}. It is important to notice that two materials with the same stress-strain curve may have similar values of l_{ch} but differently shaped tension softening curves. Thus it is not possible to use l_{ch} as a comparison between two materials whose $\sigma-\delta$ curves show large differences in shape. For the materials used in this program all the $\sigma-\delta$ curves have approximately similar bilinear shapes (Fig. 4) and so the use of l_{ch} as a parameter which characterizes changes in the tension softening behavior is adopted. Lower values of l_{ch} indicate more brittle type behavior and a $\sigma-\delta$ curve which descends quickly as the crack opens. Using a value for f_t of 2.6 MPa and the values of J_c and E given in Tables 2 and 4, l_{ch} for each volume fraction (age 14 days) was calculated as:

0% - 219 mm; 2% - 909 mm;
1% - 523 mm; 3% - 1241 mm.

These values indicate the significant effect of fibers on the material characteristic length. A typical l_{ch} value for ordinary concrete would be about 300 mm [6]. The objective is to relate the shear and flexural strengths to the characteristic length.

Shear Strength

In conventional structural design shear strength has been predicted by means of empirical formulae based on experimental data obtained from laboratory-sized specimens. These formulae tend to overestimate the strength of deep beams because of an observed reduction in strength as beam depth increases. It has been suggested [4, 5, 6, 7, 8] that shear strength should be examined from a fracture mechanics viewpoint. Gustafsson [7] used the "fictitious crack model" and finite element analysis to study shear behavior. He assumed that a crack initiates at the bottom of a beam and propagates towards the load point along a predetermined path. The concrete elements on the crack path were assumed to deform according to a linear σ–ε curve up to the tensile strength and then follow a post peak bilinear σ– δ curve as shown in Fig. 20, while the elements outside the fracture zone were assumed linear elastic. Rebars were simulated with one-dimensional elements whose bond strength was a function of slippage relative to the surrounding concrete element. Dowel action and aggregate interlocking were not considered during the theoretical analysis. The assumed failure criterion is shown in Fig. 17. In this analysis f_c/f_t was assumed equal to 10 for all concrete qualities. This gave a relationship between the shear strength normalized by the tensile strength, f_v/f_t and the depth normalized by the characteristic length, d/l_{ch}.

Fig. 18 shows the theoretical relationship between f_v/f_t and d/l_{ch} for a span depth ratio of 3 and a steel reinforcement ratio, ρ, of 2%. Also shown are the results of our shear beam tests which apply to a span depth ratio of 2. A direct comparison of these results is not possible because of differences in the span depth ratio, the crack propagation pattern and the f_c/f_t ratio. In the experiments the f_c/f_t ratio decreased approximately from 20 to 15 as the fiber volume increased, which differs from the assumed value of 10 used in the analysis. Also there is some difference between the assumed tension-softening curves and the actual curves as outlined in Fig. 20. However according to Fig. 17 an increase in f_c/f_t should give rise to an increase in shear strength as should a reduction in the span depth ratio. Thus the relative positions of the two curves in Fig. 18 appear to be correct.

Energy is absorbed during cracking by dowel action in the rebars, frictional sliding between the crack faces and crack propagation. Energy absorbed in the fracture process zone as characterized by the area under the tension-softening curve, is probably quite small compared to that absorbed by the first two

mechanisms given above for a beam of this size. Thus large changes in the shear strength are not really expected. This may not be the case, however, for lightly reinforced sections or for deeper beams where the tension-softening behavior would most likely be more important.

Fig. 19 shows qualitatively a possible distribution of the shear resistance as a function of load point displacement among the three components listed above. Before peak load, deformations are not large enough to develop the first two resistance components fully. The third component, however, has maximum effect when the first crack appears and its effect gets much smaller as the maximum load is approached. This explains why the tension-softening curve has much greater influence on the first cracking strength than on the ultimate strength of the beam.

Using assumptions by Hillerborg [21] it is possible to estimate the sensitivity of the shear strength to changes in various material parameters. He assumed that the following relationship existed between the f_v/f_t and d/l_{ch} ratios.

$$\ln(f_v/f_t) = A - B\ \ln(d/l_{ch}) \tag{8}$$

where A and B are functions of structural properties such as reinforcement ratio, shear span to effective depth ratio, loading configuration, etc. This assumption is limited to small changes in the material properties and so A and B may be functions of these properties also.

In the shear tests the beam depth and f_t were unchanged and so differentiation of Eq. (8) results in

$$\frac{df_v}{f_v} = B\frac{dE}{E} + B\frac{dJ_c}{J_c} \tag{9}$$

which gives the sensitivity of shear strength to changes in E and J_c. In order to estimate these sensitivities the differences of each value between two adjacent volume fractions, 0% and 1%, were substituted into Eq.(10) and B was calculated as approximately 0.05. This says that for a 100% increase in G_F the expected increase in f_v is approximately 5% for the beam size tested.

A limited amount of experimental data on the factors which influence shear strength of FRC beams is available. In a recent study of the use of steel fibers as shear reinforcement [22], the effects of longitudinal reinforcement ratio and shear span to effective depth ratio on the shear strength were investigated. It was found that the effectiveness of dowel resistance of longitudinal reinforcement increased with the volume fraction of steel fibers and also that the shear strength increased 47% when the span to effective depth ratio was reduced from 3 to 2. This trend is similar to that found for ordinary reinforced concrete beams but is of much greater magnitude.

These phenomena can be explained in terms of the resistance components outlined in Fig. 19. An increase in the reinforcement ratio leads to greater shear resistance due to dowel action. As the shear span is reduced the crack is more steeply inclined and thus the vertical component of shear friction between the crack faces is increased leading to a larger overall shear resistance. Also as the crack becomes steeper the vertical component of tensile stresses transferred across the fracture zone will be reduced resulting in a smaller influence of the tension softening curve on the shear strength as the span is reduced. This agrees with the results presented in Fig. 18.

Flexural Strength

The strength of concrete in flexure is of practical importance in applications such as paving slabs, road slabs, airfield runways, factory floors, tunnel linings, concrete pipes, roof tiles and also when calculating the cracking load and deflection of reinforced concrete members. However, when calculating the flexural strength in the laboratory it has been found to depend on the specimen depth and the loading configuration. Conventional theories have attempted to explain these phenomena using arguments such as "the highly stressed volume" [23], "the weakest link in the chain", and also by considering the effect of differential shrinkage strains in the specimen. While each of these qualitative arguments makes sense, their application to design is limited.

Hillerborg et al [18] and Gustafsson [7] have used the "fictitious crack model" and finite element analysis to develop a relationship between two dimensionless ratios f_f/f_t and d/l_{ch}. The stress-strain curve was assumed linear. At small loads the stress distribution is linear. When the tensile stress is reached in the bottom fiber a fracture zone starts developing and this material behavior is governed by the tension-softening curve. Initially the bending moment increases as the fracture zone develops, it reaches a maximum and then starts to decrease. Theoretical analyses [20] indicated that the shape of the σ–δ curve for given

values of f_t, E and G_F has a significant influence on the flexural strength. At ultimate load a traction-free crack has not started to propagate and thus while the initial part of the σ–δ curve is very important the relationship for large values of δ often has no influence on the ultimate strength. The theoretical relationships developed [18,7] were based on assumed linear or bilinear tension softening curves. Fig. 20 shows a comparison between the assumed curves and the deduced curve for $V_f = 2\%$.

The deduced f_f/f_t versus d/l_{ch} relationships based on assumed linear and bilinear tension softening curves are presented in Fig. 21. A third relationship is presented which takes account of initial shrinkage stresses assumed to be parabolically distributed along the depth of the beam and equal in magnitude to the tensile strength at the upper and lower edges of the beam [7]. Also shown in this figure are the experimental results from the flexural tests.

Since J_c was only measured at 14 days the value of l_{ch} at 60 days corresponding to the small beam flexure tests had to be estimated. Relations between fracture mechanical properties and concrete age [6] used to do this were as follows:

J_c (60 days) = 1.1 J_c (14 days)
E (60 days) = 1.06 E (14 days)

The splitting tension test results were used for f_t. The calculated l_{ch} for each volume fraction (age 60 days) was as follows:

0% - 135 mm; 2% - 512 mm;
1% - 308 mm; 3% - 685 mm.

This large drop in l_{ch} with age is consistent with experimental results presented in [6].

There are some differences between the assumptions underlying the theoretical curves and the actual experimental conditions. The theoretical relationships are based on an average cross section with average stress-strain and tension-softening relationship. The small beam relationship was developed using the splitting tensile strength of a specified cross section which may be expected to be close to the strength of the average section. The flexural strength, however, was calculated using four-point bending specimens which yield the strength of the weakest section along the central part of the beam. Thus the experimental f_f/f_t values are expected to be less than the theoretical predictions as is the case.

The results for the large beams follow quite closely the predicted values based on the assumed initial stress distribution. It is possible that shrinkage stresses were developed in these specimens during the curing process. Notice that the small beams were cut from the central part of other specimens and so shrinkage would not have been important. Also, shrinkage would have a negligible effect on low modulus fibers and so where initial stresses are a problem it is expected that the beneficial effect of fibers is much more pronounced. If initial stress corresponding to the tensile strength exists at the bottom of the beam then this material starts to soften immediately when load is applied giving rise to a much greater influence of the σ–δ curve on the structural behavior than if no initial stresses existed. The large beam test results support this idea. Due to the effects of age, loading rate and initial stresses it is not possible to estimate quantitatively the effect of changing the beam depth on the f_f/f_t ratio except to say that there appears to be a significant increase in f_f as the depth is reduced.

Theoretical bending strengths of notched beams as a function of the ligament size divided by characteristic length, assuming a bilinear σ–δ curve as in Fig. 20, have been presented by Hillerborg [24]. A comparison of these predictions with the results obtained from the notched beam tests as outlined in Table 1 is given in Fig. 22. The experimental results show a greater sensitivity of bending strength to changes in l_{ch} than that predicted theoretically by the "fictitious crack model". Initial shrinkage stresses may explain this trend.

CONCLUSION

The influence of the tension-softening curve on the ultimate load carrying capacity of structures where tensile stresses are critical was examined. By using low volume fractions of low modulus acrylic fibers it was possible to significantly change the tension-softening curve without changing the pre-peak stress-strain curve. These fibers caused some reduction in the compressive strength depending on how well the material was compacted. It is believed that by using good compaction techniques and adequate amounts of superplasticizer, this strength reduction could be minimized.

The fracture energy value, characterized by the area under the tension-softening curve, shows a significant increase with fibers, being of the order of

570% when a volume fraction of 3% is used. Also by using J_c rather than G_F to characterize the fracture energy difficulties associated with the effects of beam size and energy losses outside the fracture zone can be avoided.

The shear strength of longitudinally reinforced beams showed a modest increase of 12% when the characteristic length was increased by 460%. However, the stress at which a first visible crack appeared showed a much greater increase of 50%.

The flexural strength of unreinforced beams, 114.3 mm deep and in which significant initial shrinkage stresses were expected showed a large increase (80%) when the value of l_{ch} was increased (460%). The strength increase for small beams which probably had negligible initial stresses was much less (30%) for an l_{ch} change of (400%).

Traditional strength theories based solely on the pre-peak stress-strain curves cannot predict the capacity of structures subjected to tensile stresses if a fracture zone starts to develop prior to maximum load. In such a case it is necessary to also use the tension-softening curve to predict ultimate strength of the structure. Fracture mechanics parameters such as fracture energy and characteristic length are just as important as tensile and compressive strength in determining the behavior of structures made of a brittle material such as concrete.

ACKNOWLEDGEMENT

The authors would like to thank K. Chong and Y. Wang for the many helpful discussions in the course of this work. Funding from the National Science Foundation and the Shimizu Corporation is gratefully acknowledged.

REFERENCES

1. Wang, Y., Backer, S., Li, V.C., "An Experimental Study of Synthetic Fiber Reinforced Cementitious Composites," *Journal of Materials Science* 22, 1987, pp.4281-4291.

2. Li, V.C., Backer, S., Wang, Y., Leung, C.K.Y., Yamanobe, K., "Tensile Failure Mechanisms and Mechanical Properties of Fiber Reinforced Concrete," *Proceedings of the International Symposium on Fiber Reinforced Concrete*, Madras, India, Dec. 1987.

3. Li, V.C., Liang, E., "Fracture Processes in Concrete and Fiber Reinforced Cementitious Composites," *ASCE Journal of Engineering Mechanics*, Vol. 112, No. 6, June 1986, pp. 566-586.

4. Shioya, T., Iguro, M., Nojiri, Y., Akiyama, H., Okada, T., "Shear Strength of Large Reinforced Concrete Beams," Intended for Symposium Volume "Application of Fracture Mechanics to Cementitious Materials and Structures," 1988.

5. Hillerborg, A., "Fracture Mechanics and the Concrete Code," Intended for Symposium Volume "Application of Fracture Mechanics to Cementitious Materials and Structures," 1988.

6. Petersson, P.E. "Crack Growth and Development of Fracture Zones in Plain Concrete and Similar Materials," Report TVBM-1006, Div. of Building Materials, Lund Institute of Technology, Sweden,1981.

7. Gustafssen, P.J., "Fracture Mechanics Studies of Non-yielding Materials Like Concrete," Report TVBM 1007, Div. of Building Materials, Lund Institute of Technology, Sweden, 1985.

8. Bazant, Z.P., Sener, S., Prat, P.C., "Fracture Mechanics Size Effect and Ultimate Load of Beams under Torsion," Intended for symposium volume, "Application of Fracture Mechanics to Cementitious Materials and Structures," 1988.

9. Gopalaratnam, V.S., Shah, S.P., "Tensile Fracture of Steel Fiber Reinforced Concrete," *Journal of Engineering Mechanics*, Vol. 113, No. 5, May 1987, pp. 635-652.

10. Li, V.C., *Applications of Fracture Mechanics to Cementitious Composites*, Ed. S.P. Shah, p. 431, Martinus Nijhoff Publishers, Dordrecht, 1985.

11. Li, V.C., Chan, C.M., Leung, C.K.Y., "Experimental Determination of the Tension Softening Relations for Cementitious Composites," Accepted for publication, *Cement and Concrete Research,*1987.

12. Leung, C.K.Y., Li, V.C., "Determination of Fracture Toughness Parameter of Quasi Brittle Materials with Laboratory-size Specimens," In press, J. of Materials Science, 1988.

13. Rice, J.R., "A Path Independent Integral and the Approximate Analysis of Strain Concentrations by Notches and Cracks," *Journal of Applied Mechanics*, 1968, pp.379-386.

14. Proposed RILEM recommendation, "Determination of the Fracture Energy of Mortar and Concrete by Means of Three-point Bending Tests on Notched Beams," Division of Building Materials, Lund Institute of Technology, Sweden, 1982.

15. Horvath, R. and Persson, T., "The Influence of the Size of the Specimen on the Fracture Energy of Concrete," Report TVBM-5005, Div. of Building Materials, Lund Institute of Technology, Sweden, 1984.

16. Lim, T.Y., Paramasivam, P., Lee, S.L., "Bending Behavior of Steel-Fiber Concrete Beams," *ACI Structural Journal*, Vol.84, No. 6, Nov.-Dec. 1987, pp. 524-536.

17. Neville, A.M., *Properties of Concrete*, Third Edition, A Pitman International Text, Publ. 1981.

18. Hillerborg, A., Modeer, M., Petersson, P.E., "Analysis of Formation and Crack Growth in Concrete by means of Fracture Mechanics and Finite Elements," *Cement and Concrete Research*, Vol. 6, 1976, pp.773-782.

19. Hillerborg, A., "A Model for Fracture Analysis," Report TVBM-3005, Div. of Building Materials, Lund Institute of Technology, Sweden, 1978.

20. Modeer, M., "A Fracture Mechanics Approach to Failure Analyses of Concrete Materials," University of Lund, Sweden, 1979.

21. Hillerborg, A., "Determination and Significance of the Fracture Toughness of Steel Fiber Concrete," Steel Fiber Concrete, US-Sweden Joint Seminar (NSF-STU), June 1985.

22. Narayanan, R., Darwish, I.Y.S., "Use of Steel Fibers as Shear Reinforcement," *ACI Structural Journal*, Vol. 84, No. 3, May-June 1987, pp. 216-227.

23. Torrent, R. J., Brooks, J.J., "Application of the Highly Stressed Volume Approach to Correlated Results from Different Tensile Tests of Concrete," *Magazine of Concrete Research*, Vol. 37, No. 132, September 1985.

24. Hillerborg, A., "Influence of Beam Size on Concrete Fracture Energy Determined According to a Draft Rilem Recommendation," Report to Rilem TC50-FMC, Div. of Building Materials, Lund Institute of Technology, Sweden, 1985.

TABLE 1--G_F AND f_f(net) VALUES FROM NOTCHED BEAM TESTS

Beam	G_F (N/m)	self-wt correction (N/m)	f_f net (MPa)	Beam	G_F (N/m)	self-wt correction (N/m)	f_f net (MPa)
OA	96	15.7	2.13	2A	421	55.6	3.37
OB	86	11.1	2.16	2B	430	53.6	4.04
OC	78	11.6	2.15	2C	293	42.0	2.78
OD	122	18.9	2.43	2D	414	57.0	3.23
OE	49	10.5	1.56	2E	397	56.7	3.78
OF	52	8.5	2.03	2F	442	54.2	4.17
OG	65	11.1	2.33	2G	371	55.7	4.07
OH				2H	424	66.9	4.07
1A	198	30.3	2.63	3A	595	76.0	4.49
1B	212	25.2	3.14	3B	619	71.4	4.95
1C	188	27.0	2.70	3C	580	64.4	4.26
1D	196	31.7	2.63	3D	630	68.5	5.00
1E	242	33.1	3.46	3E	653	78.6	5.16
1F	217	30.9	3.11	3F	738	96.8	5.11
1G	296	34.0	4.09	3G	618	74.8	4.60
1H	212	29.3	3.04	3H	553	74.5	4.53

TABLE 2--CHARACTERISTICS OF TENSION-SOFTENING CURVE FOR EACH VOLUME FRACTION

Volume fraction (%)	f_{td} (MPa)	δ_c (μm)	J_c (N/m)	G_F total (N/m)	self-wt correction (% of total)
0	2.09	190	81	78	15.9
1	2.08	1100	205	209	14.2
2	2.01	1520	404	414	13.8
3	2.11	1340	543	607	12.0

TABLE 3--AVERAGE RESULTS OF DIRECT AND SPLITTING TENSION TESTS

V_f (%)	f_t (14-17 days) (MPa)	f_t (40-45 days) (MPa)	f_{st} (60 days) (MPa)
0	0.93	1.37	3.57
1	1.47	2.03	3.66
2	2.63	2.54	3.74
3	2.58	2.91	3.78

TABLE 4--AVERAGE COMPRESSION STRENGTH AND MODULUS OF ELASTICITY

V_f (%)	f_c (MPa)	E (GPa)
0	55.9	18.2
1	47.9	17.2
2	40.2	14.6
2c	48.3	17.1
3	35.4	14.3
3c	48.0	17.7

TABLE 5--COMPRESSIVE STRENGTH AND VOID RATIO FOR DIFFERENT AMOUNTS OF COMPACTION

V_f (%)	e (%)	f_c (MPa)
2	6.5	38.5
	5.0	37.1
2c	3.7	47.2
	2.6	49.5
	3.5	48.3
3	8.2	33.4
	8.7	34.1
	6.8	34.4
3c	3.0	48.4
	3.4	47.1
	4.4	48.4

TABLE 6--SHEAR TEST RESULTS

V_f (%)	f_{vc} (MPa)	f_v (MPa)	δ_v (mm)
0	2.45	4.53	0.74
1	3.11	4.91	0.63
2	3.64	4.94	0.64
3	3.73	5.10	0.64

TABLE 7--RESULTS OF FLEXURAL TEST

V_f (%)	Beam depth (mm)	Age (days)	Test time (min)	f_f (MPa)
0	114.3	14	12	2.15
2	114.3	14	18	3.53
3	114.3	14	20	3.88
0	51.0	60	2.5	5.35
1	51.0	65	2.5	6.00
2	51.0	64	2.5	6.20
3	51.0	63	2.5	6.98

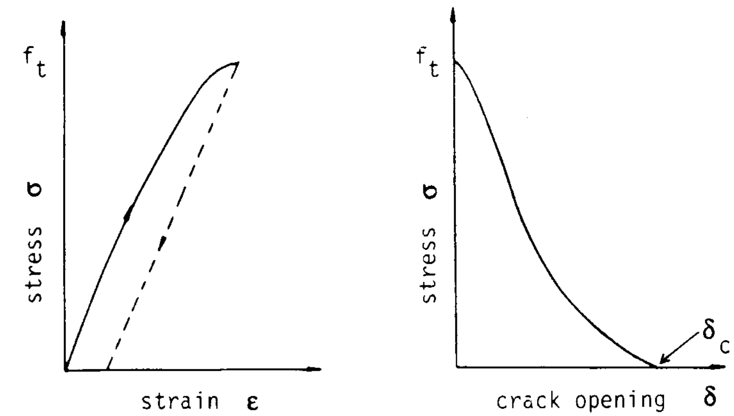

Fig. 1--Typical stress-strain and tension softening relationships for concrete

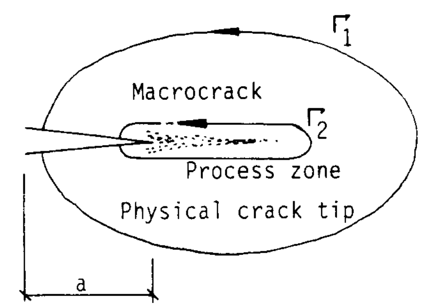

Fig. 2--J-integral contours around crack tip

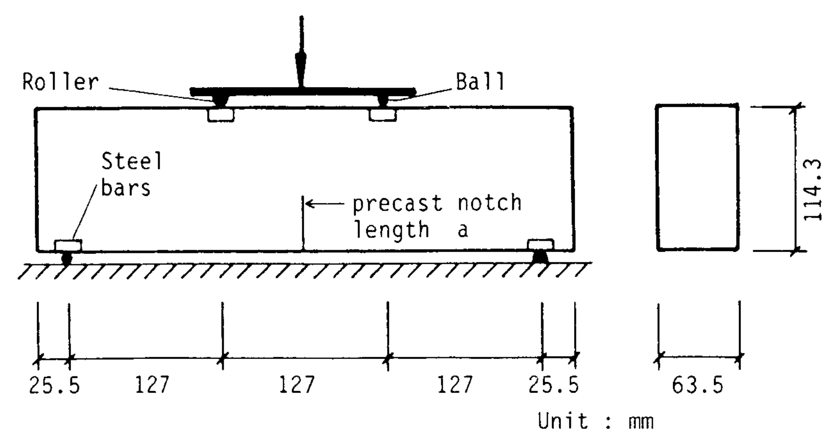

Fig. 3--Notched beam test configuration

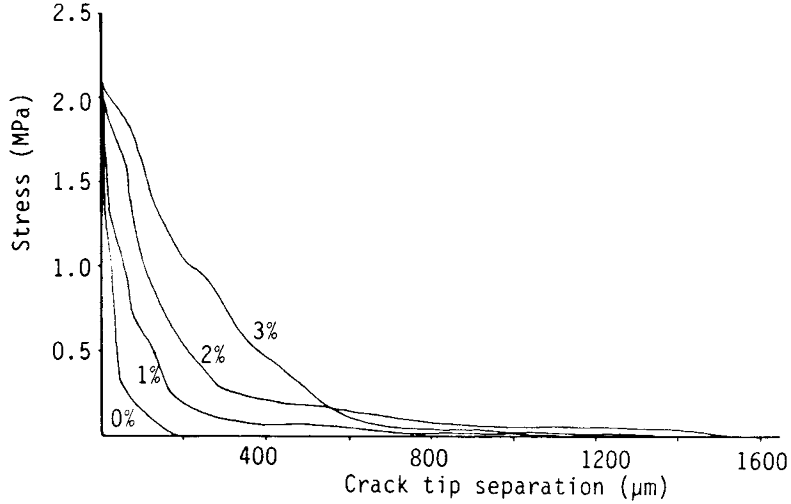

Fig. 4--Deduced tension softening curves for each volume fraction

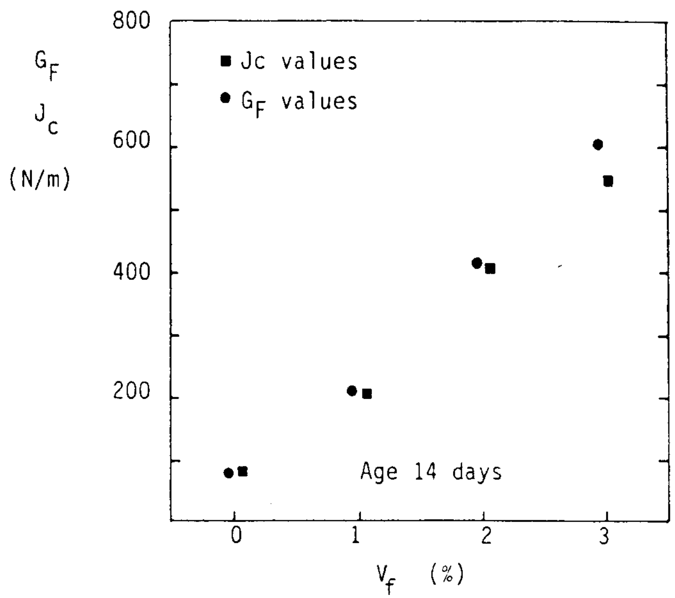

Fig. 5--Fracture energy values

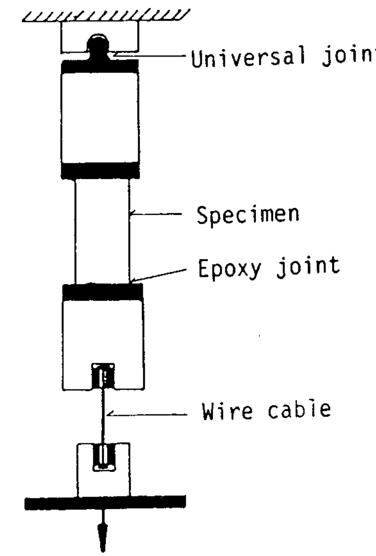

Fig. 6--Direct tension test configuration

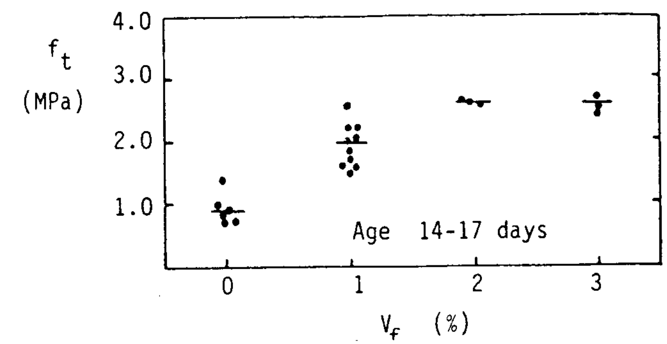

Fig. 7a--Direct tensile strength

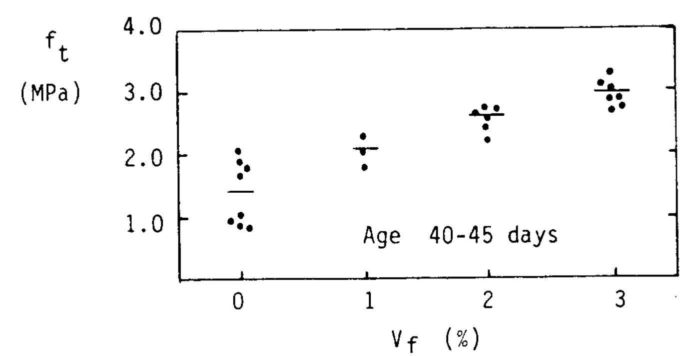

Fig. 7b--Direct tensile strength

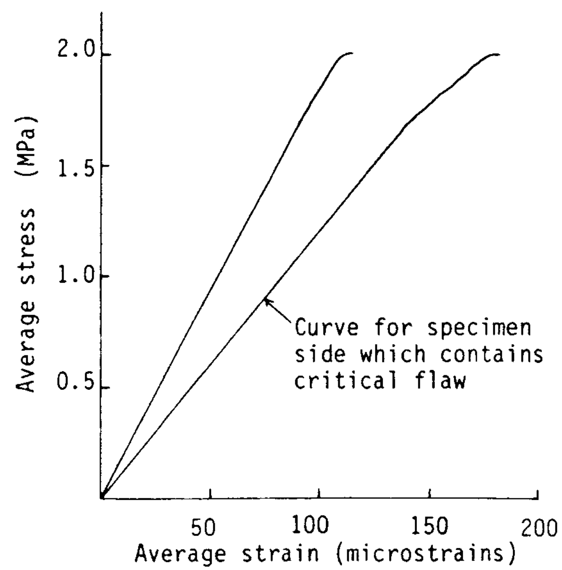

Fig. 8--Stress versus average strain measured on two sides of a direct tension specimen

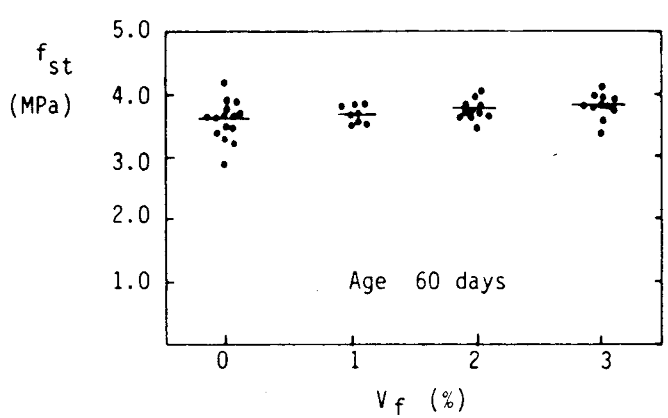

Fig. 9--Splitting tensile strength

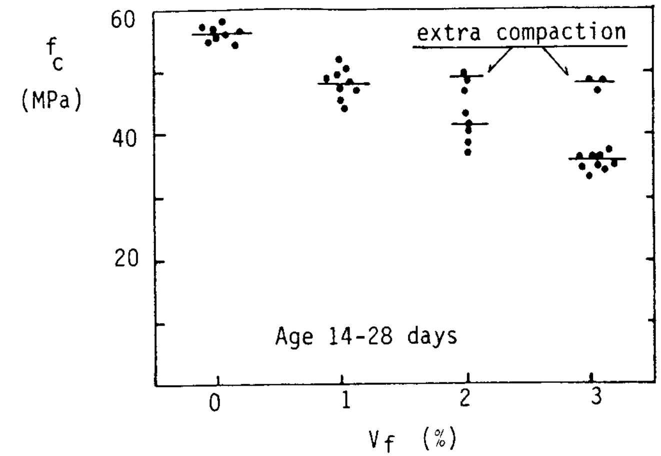

Fig. 10--Compressive strength

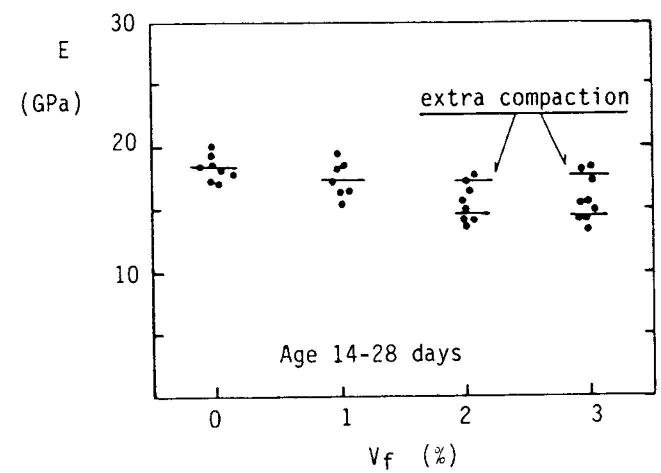

Fig. 11--Modulus of elasticity in compression

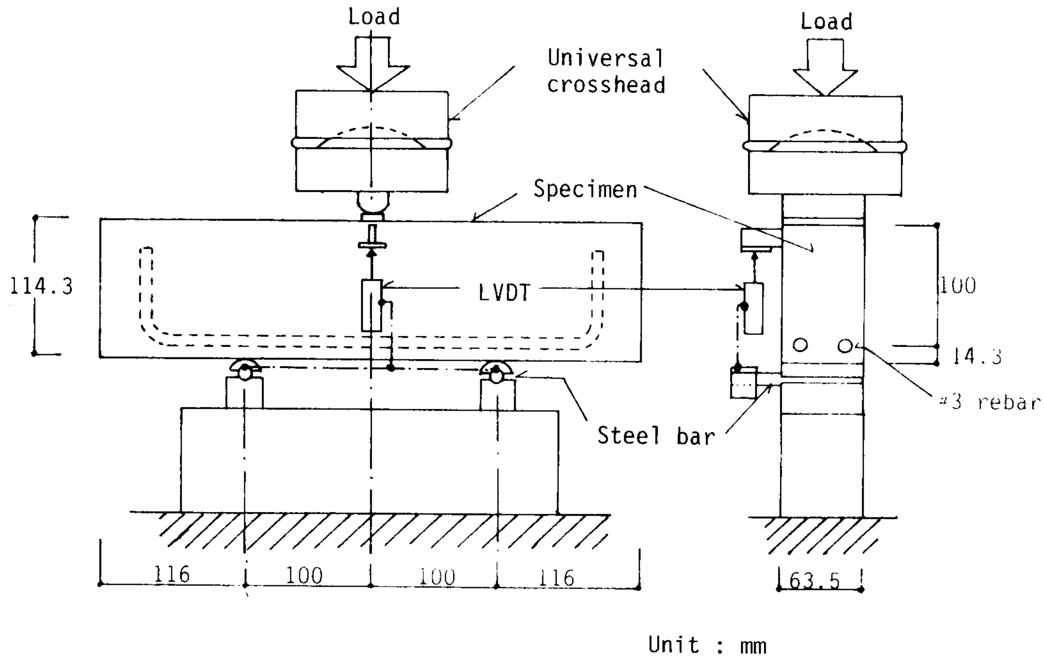

Fig. 12--Loading configuration in shear beam tests

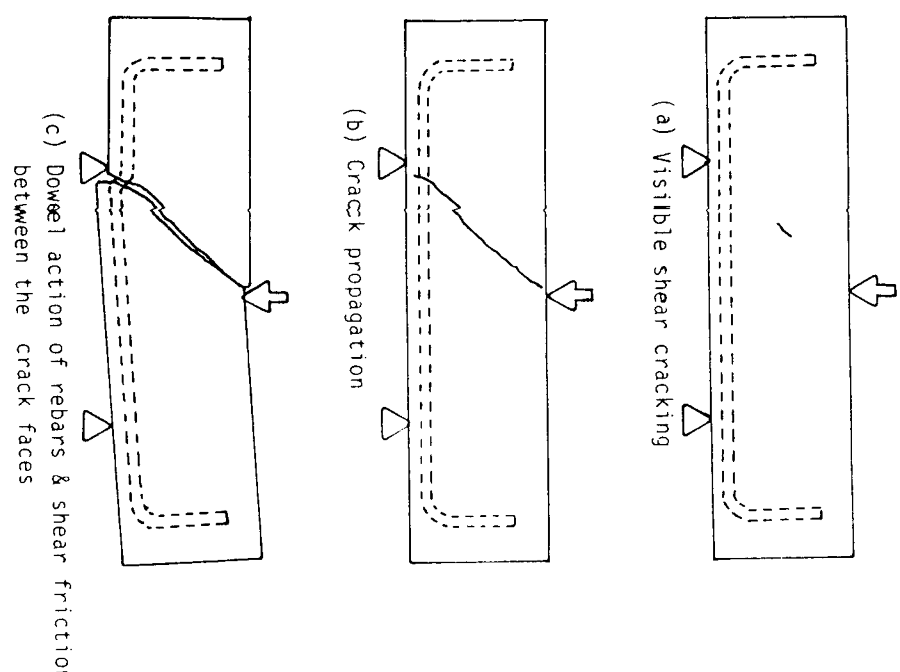

Fig. 13--Typical crack propagation patterns

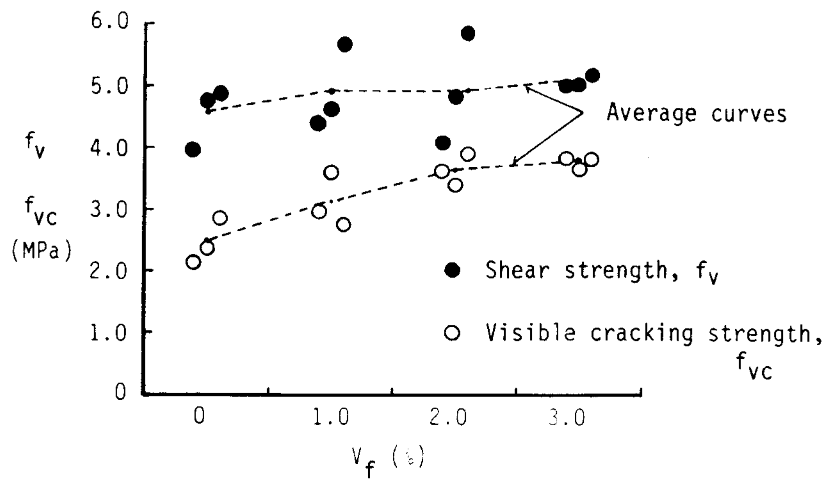

Fig. 14--Shear stress as a function of fiber volume fraction

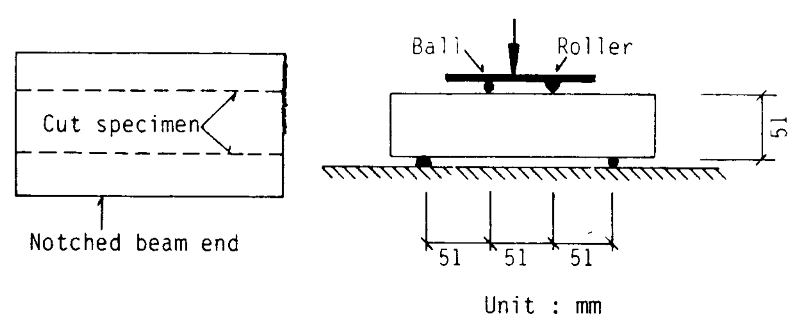

Fig. 15--Loading configuration for small beam flexural test

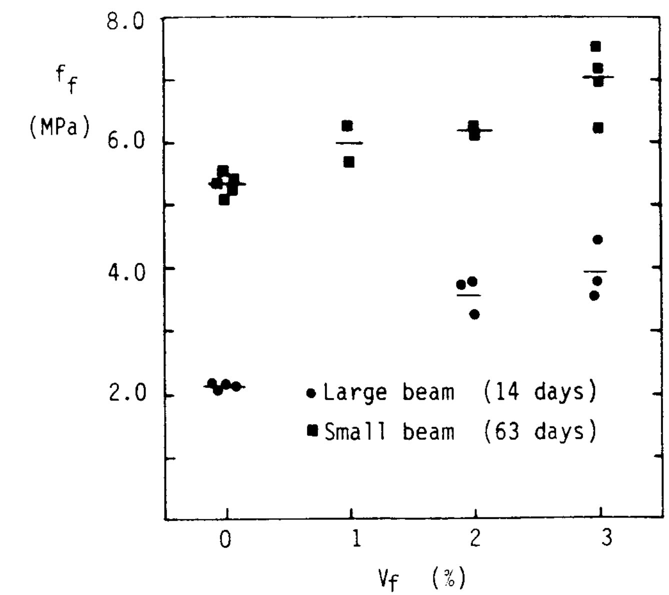

Fig. 16--Flexural strength

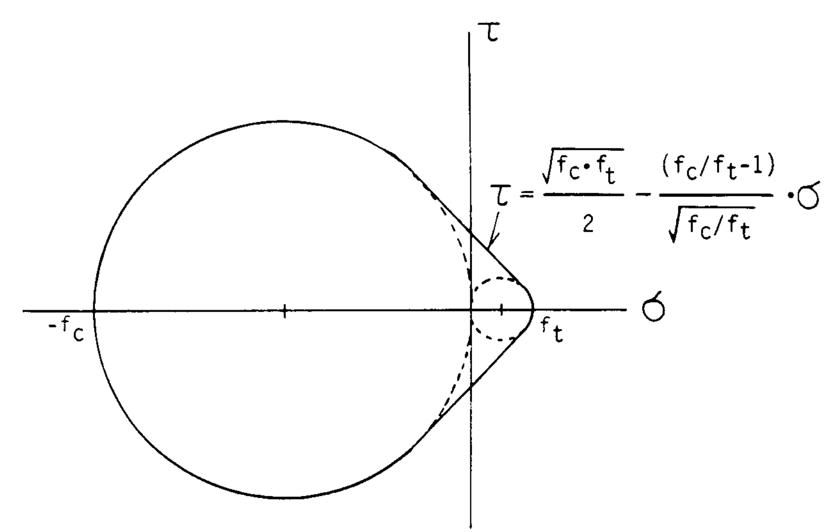

Fig. 17--Failure criterion in FRC beams

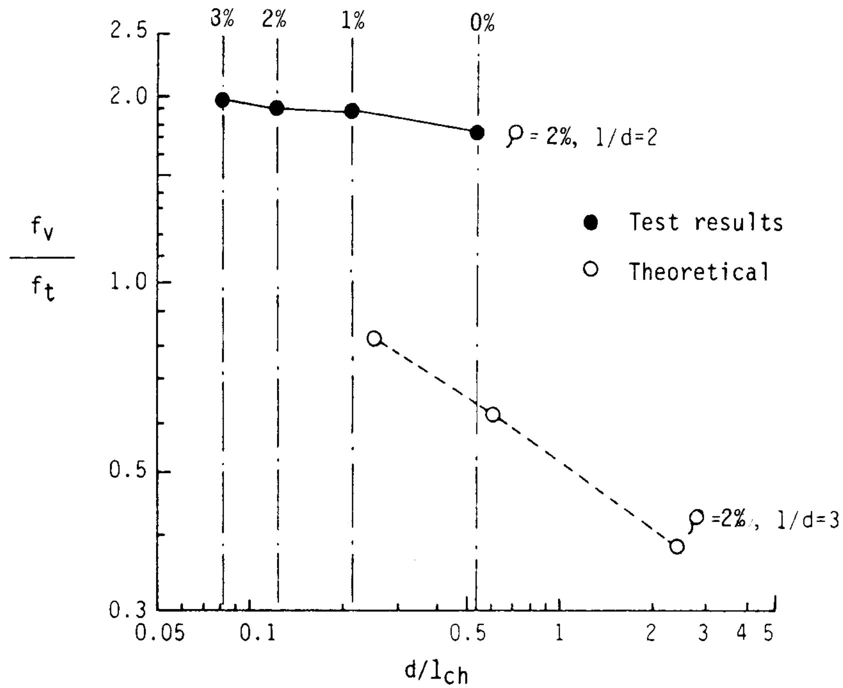

Fig. 18--f_v/f_t as a function of d/l_{ch}

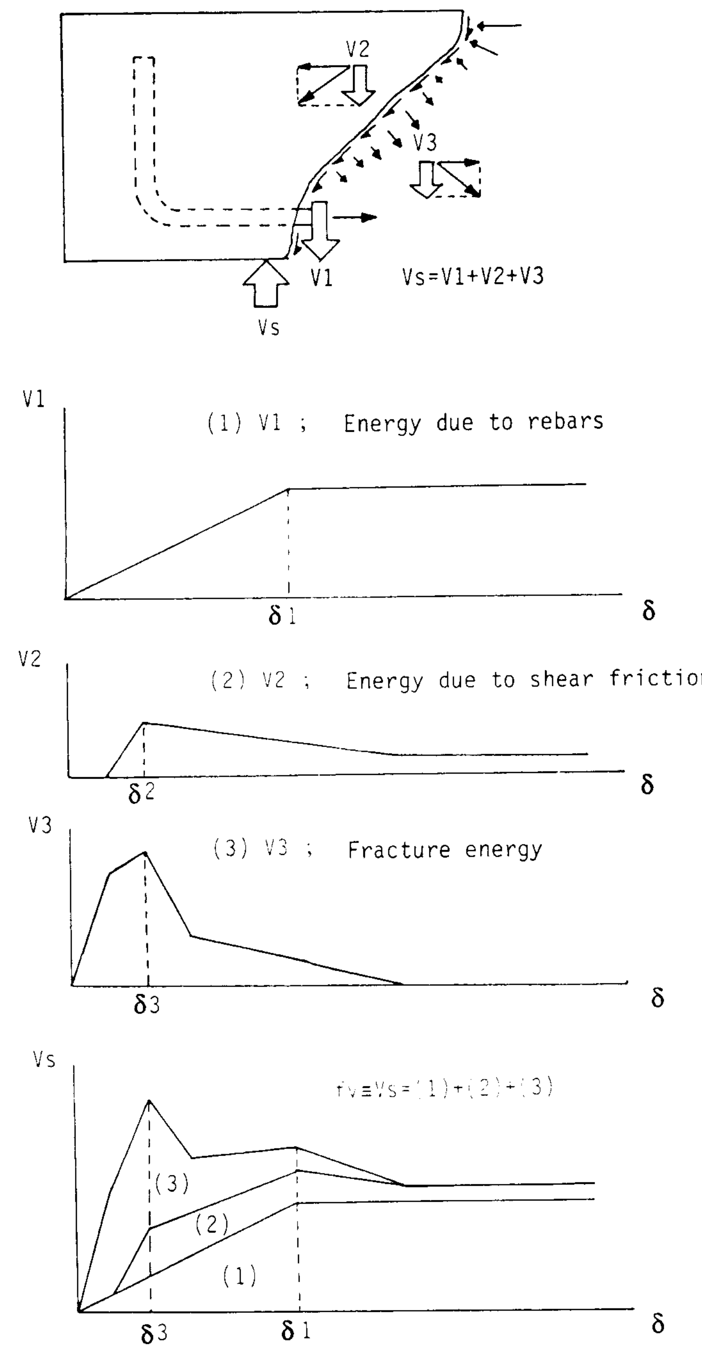

Fig. 19--Illustrative mechanism for shear transfer in FRC beams

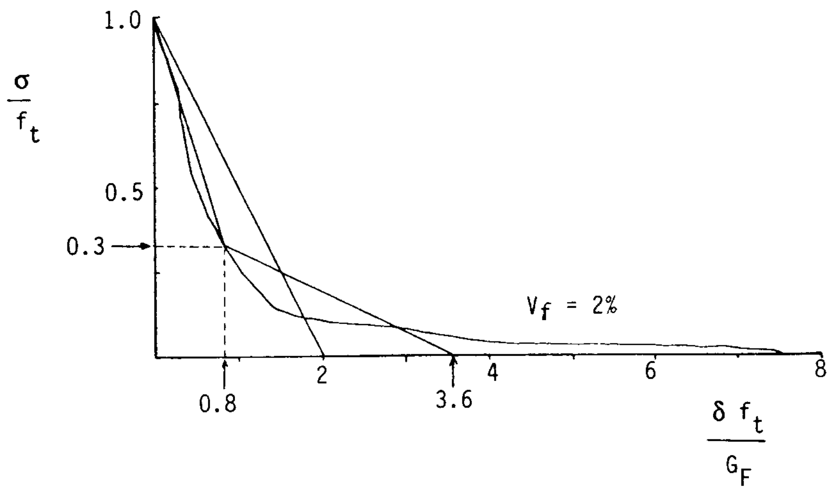

Fig. 20--Comparison between deduced and approximated tension softening curves

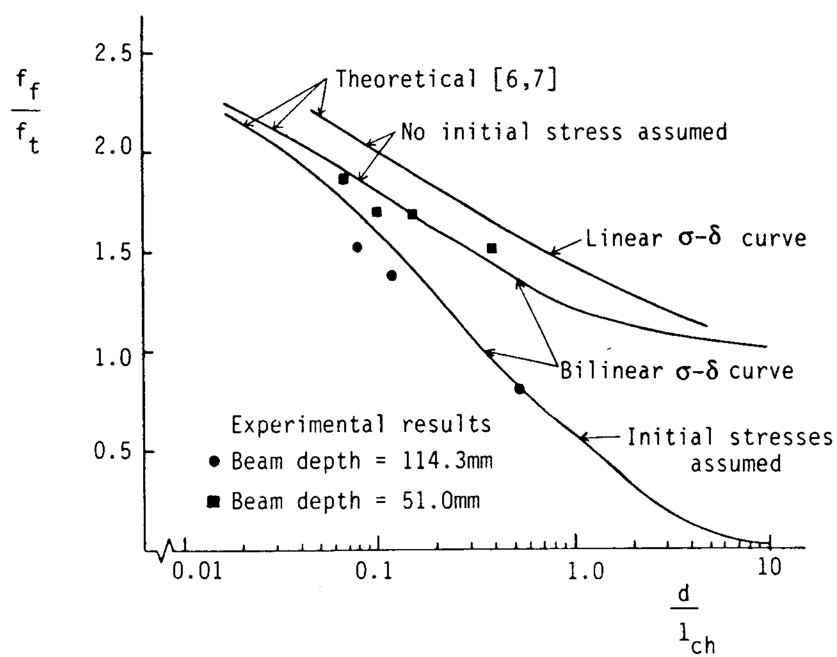

Fig. 21--Theoretical and experimental variations of the flexural strength of beams

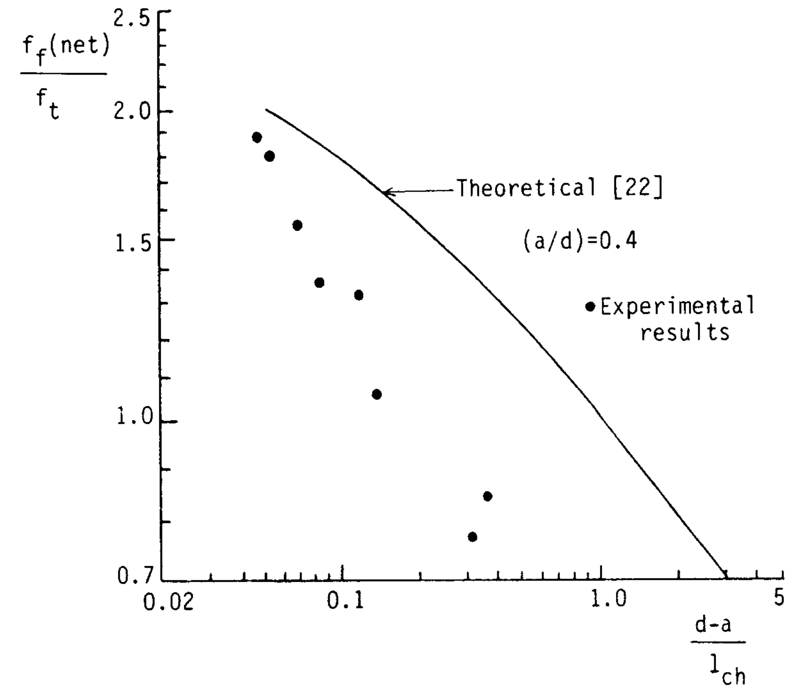

Fig. 22--Theoretical and experimental variations of the flexural strength of notched beams

APPENDIX A

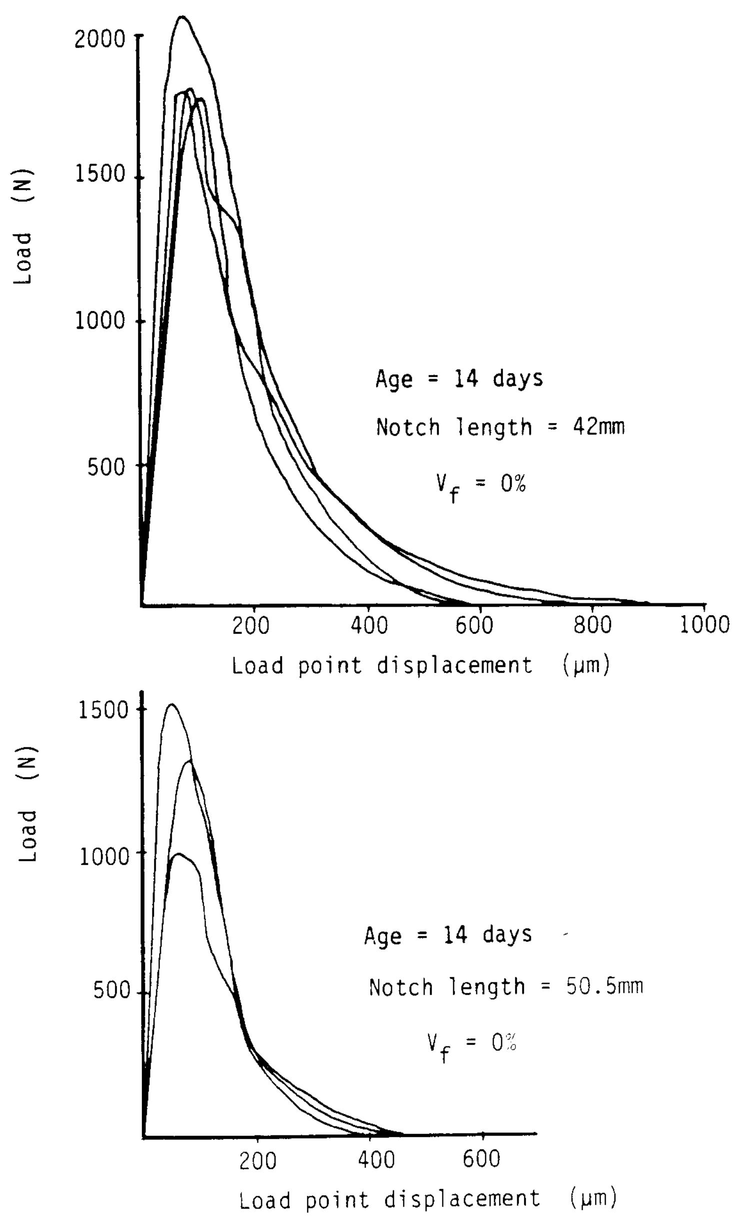

Fig. A-1--Load versus load point displacement curves for V_f = 0 percent

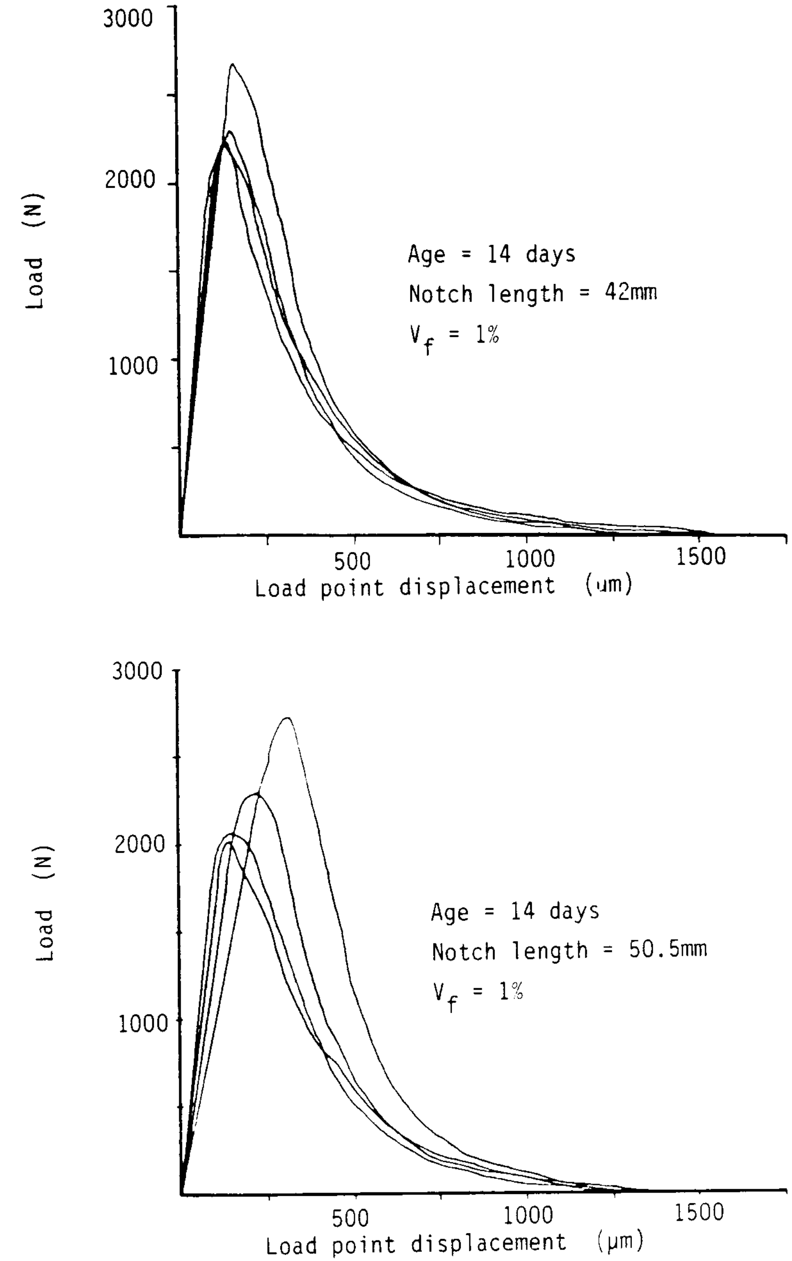

Fig. A-2--Load versus load point displacement curves for V_f = 1 percent

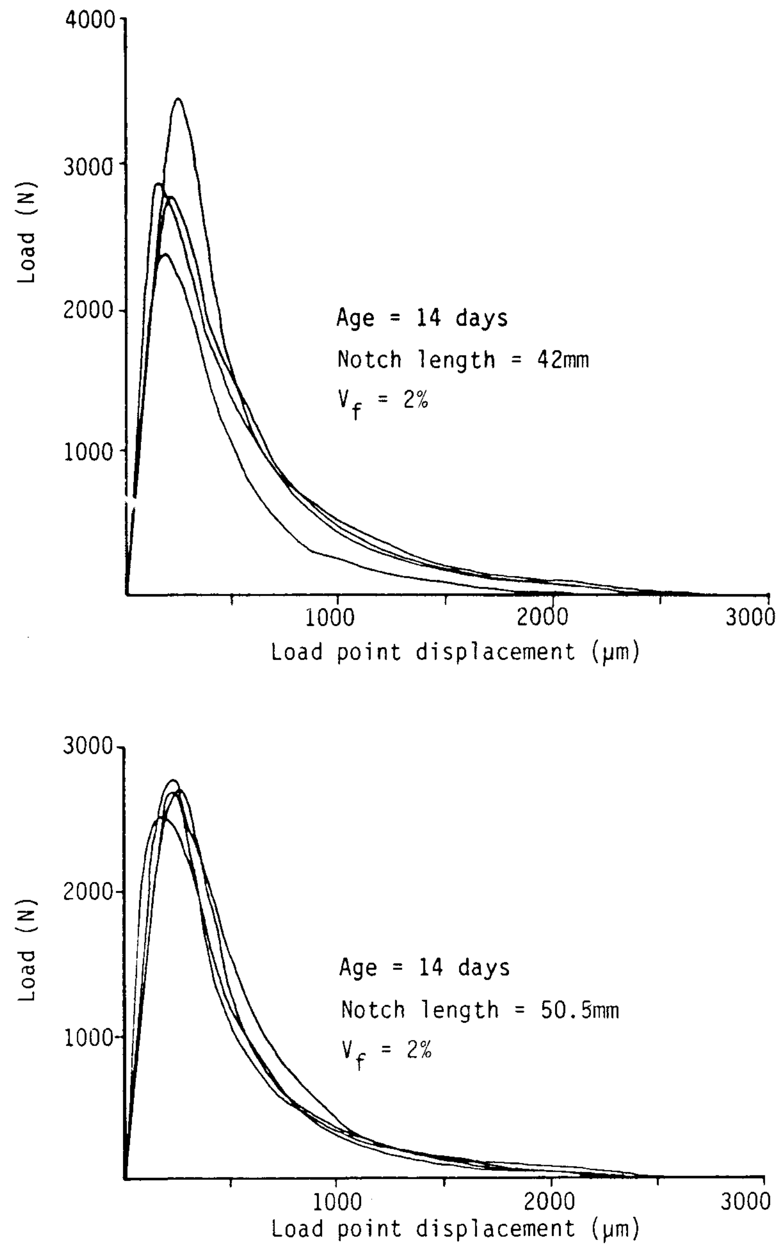

Fig. A-3--Load versus load point displacement curves for V_f = 2 percent

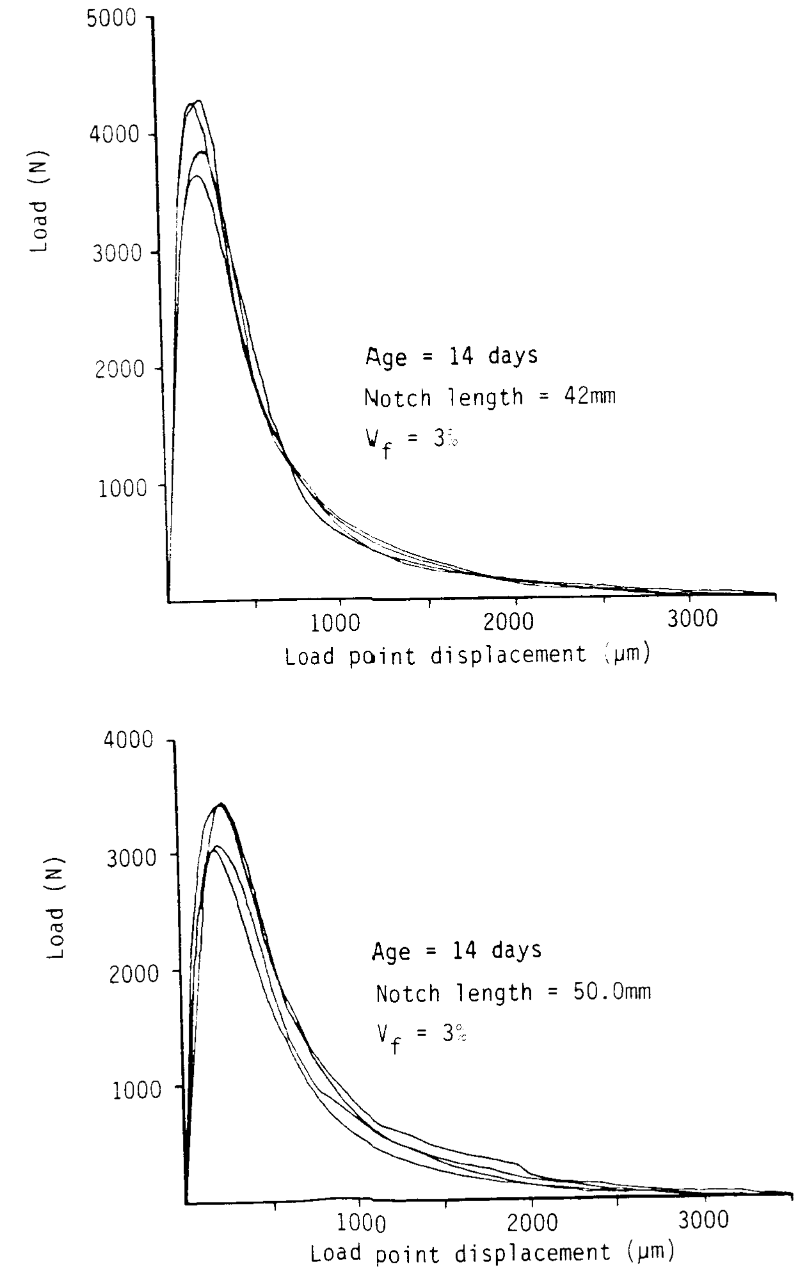

Fig. A-4--Load versus load point displacement curves for V_f = 3 percent

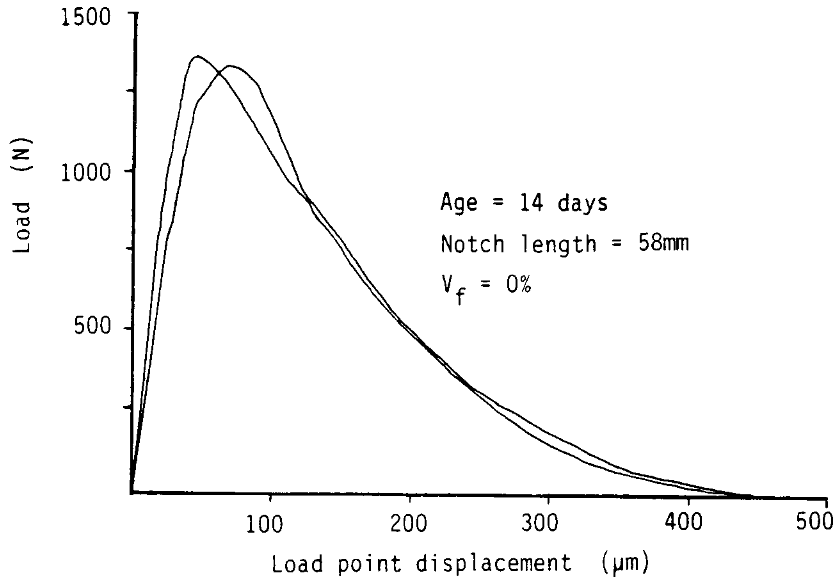

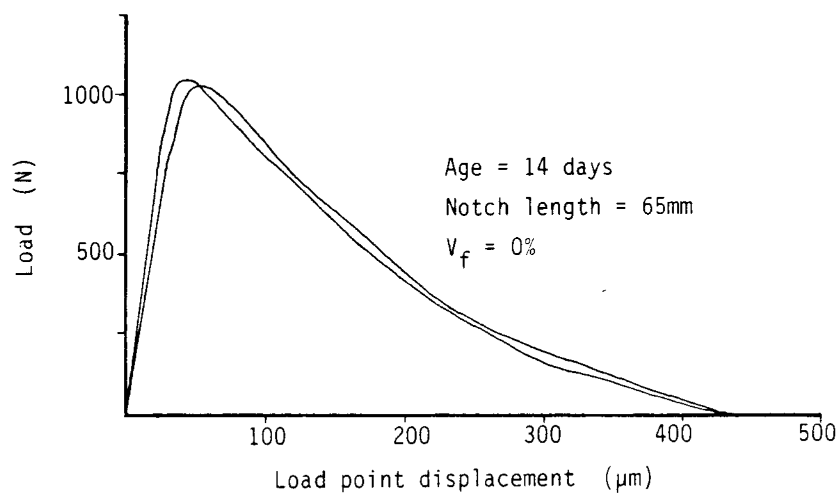

Fig. A-5--Load versus load point displacement curves for V_f = 0 percent

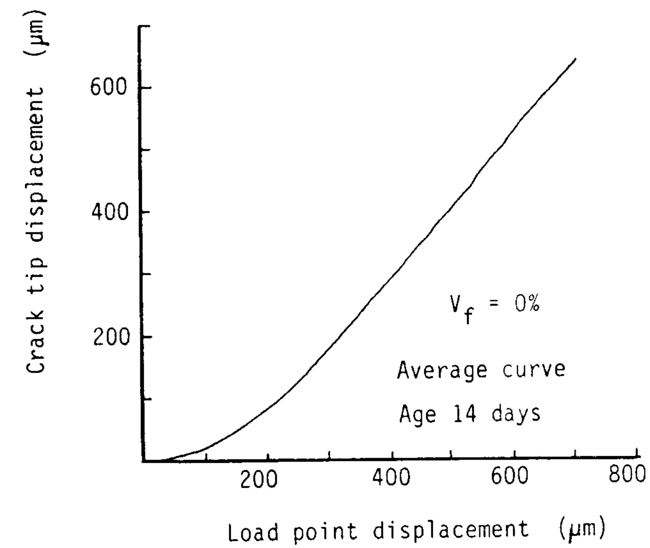

Fig. A-6--Load point displacement versus crack tip displacement for V_f = 0 percent

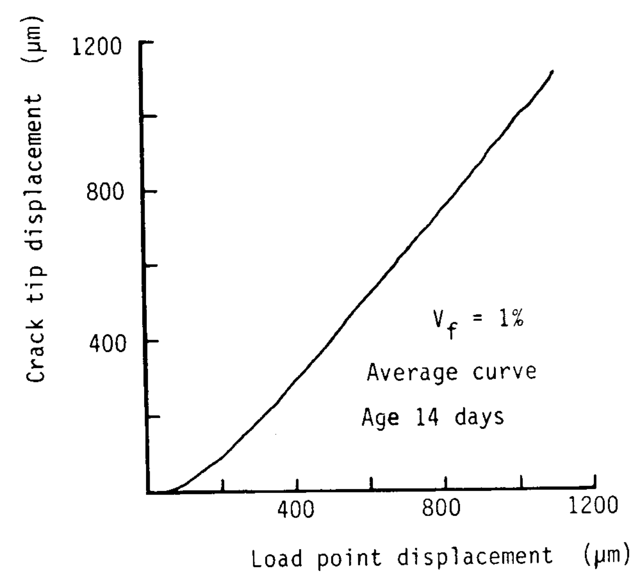

Fig. A-7--Load point displacement versus crack tip displacement for V_f = 1 percent

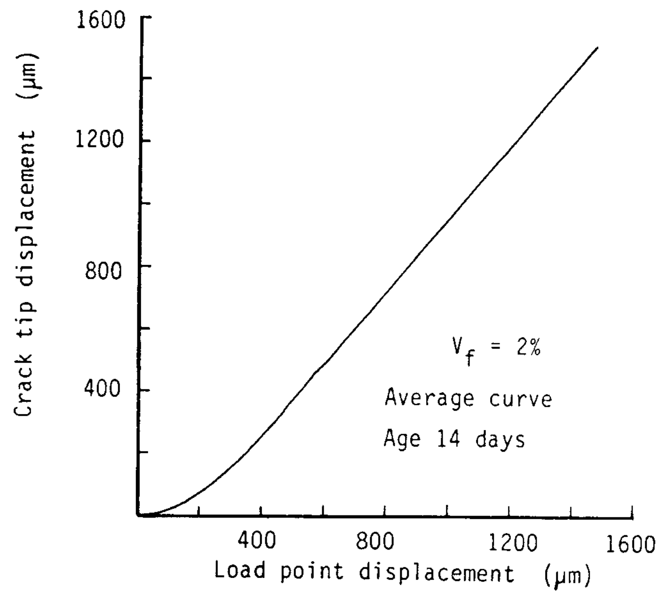

Fig. A-8--**Load point displacement versus crack tip displacement for V_f = 2 percent**

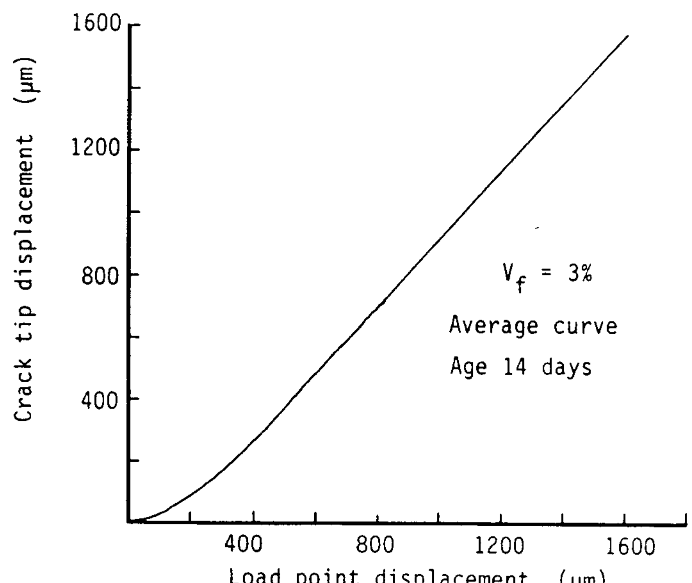

Fig. A-9--**Load point displacement versus crack tip displacement for V_f = 3 percent**

APPENDIX B

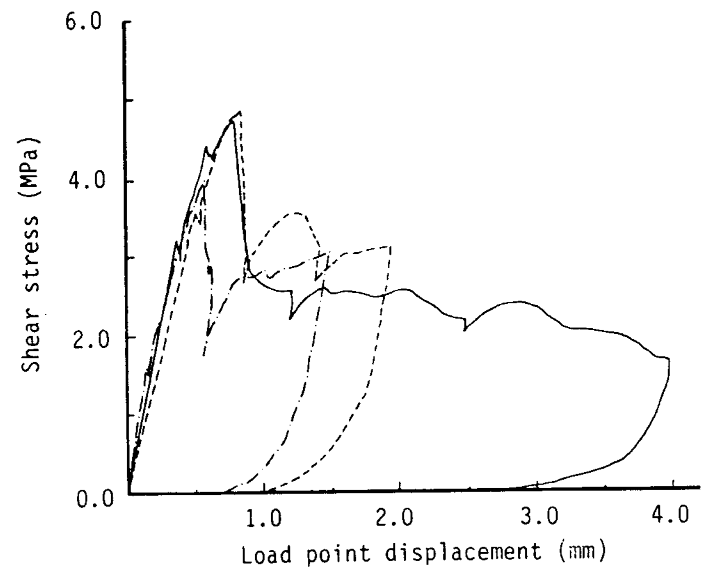

Fig. B-1--**Enveloped curves for V_f = 0 percent shear beams**

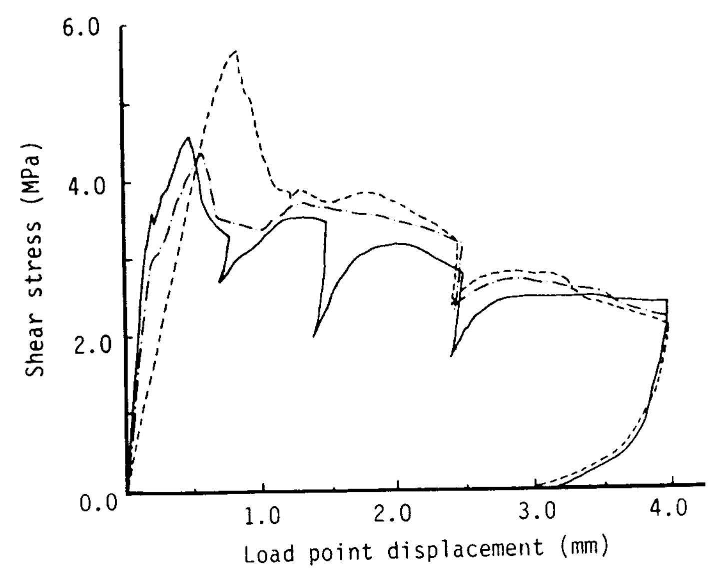

Fig. B-2--**Enveloped curves for V_f = 1 percent shear beams**

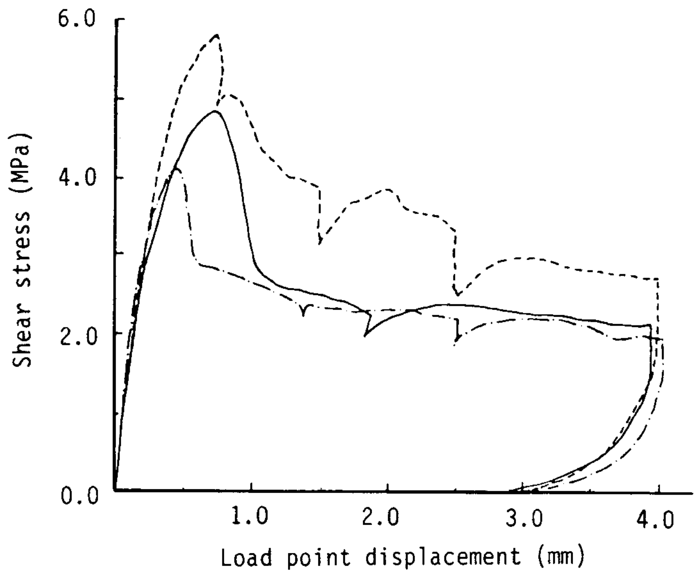

Fig. B-3--Enveloped curves for V_f = 2 percent shear beams

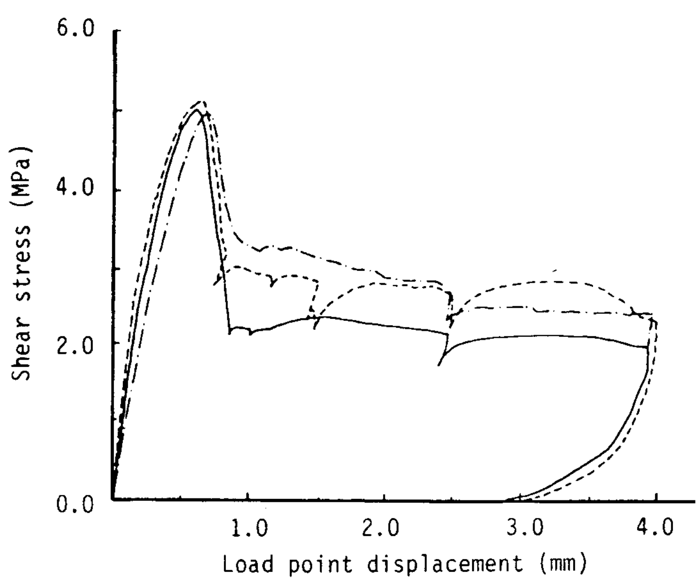

Fig. B-4--Enveloped curves for V_f = 3 percent shear beams

ADDENDUM

Additional experimental work has been performed since the completion of this manuscript. In this addendum, we include two pieces of experimental results which are pertinent to the discussion in this paper.

I. Fracture energy of synthetic FRC

In the main text of this paper, the fracture energy of acrylic FRC was reported. Fracture energy measurements of synthetic FRC based on other fiber types have since been obtained, and found to provide fracture energies which can be much higher than that of acrylic FRC. These additional results are summarized in the form of a bar chart below (Figure AD1). The fracture energies of cement, concrete and high strength aluminum alloy are included for comparison. It is clear that the fracture energy of concrete is significantly improved by mixing in a few percentage of synthetic fibers. For example, the FRC with 1% volume fraction of 0.5 inch Spectra fibers shows a factor of 60 improvement over that of plain concrete. Further, continued material engineering will likely bring about synthetic FRC with fracture energy which will approach or even surpass that of certain metallic materials.

Figure AD1 also indicates that the fracture energy of FRC is strongly influenced by fiber length. In contrast, increasing volume fraction does not necessarily bring about a higher fracture energy, as indicated by the data for 1% and 2% volume fractions of Spectra (polyethylene) FRC. These aspects will be described in future publications in greater detail in relation to the micro-mechanisms of failure of different types of synthetic FRC.

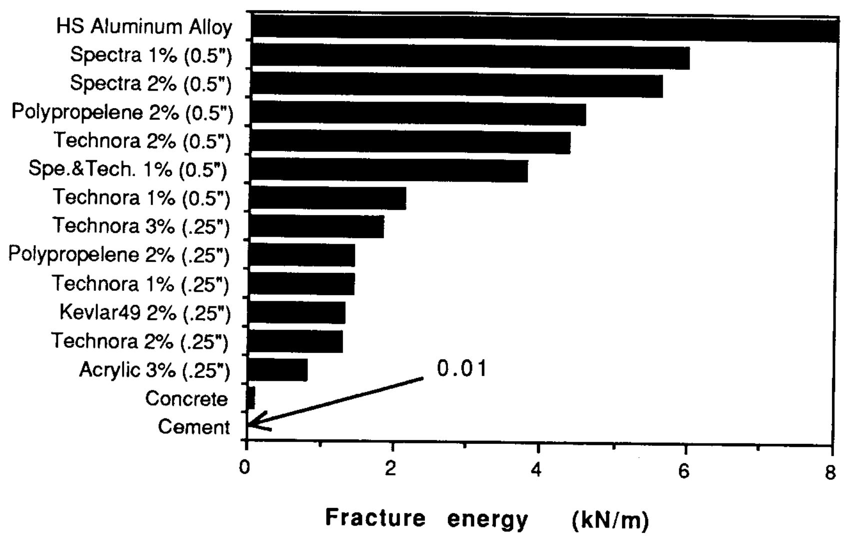

Fig. AD1--Fracture energy of synthetic FRC's

II. <u>Effect of fiber reinforcement on the shear strength of axially reinforced beams</u>

In the main text of this paper, the experimentally determined shear strength of axially reinforced beam indicates that the effect of reinforcement by acrylic fibers was only marginal. However it was felt that the small beam depth likely conceals the potential of fiber reinforcement. In retrospect, the span/depth ratio may have played a more important role since it controls the mode of beam failure. Two new series of tests with larger span/depth ratios of 3 and with depths of 4" and 6" were carried out. These new series involve the use of Kevlar 49 (aramid) fibers of 0 and 2% volume fraction. The test results are summarized in Figure AD2.

It is clear from Figure AD2 that the shear strength has improved about 300% for both beam sizes with the addition of 2% volume fraction of fibers. It was observed that the plain concrete beams fail with brittle sharp cracks which spall and leave the steel re-bars exposed as the beam was loaded to failure. With fiber reinforcement, no spalling was observed and the cracks became more tortuous. These results attest to the fact that ultimate strength in flexure and shear can be controlled by the fracture process in reinforced concrete beams. Further, the use of fibers can significantly alter the characteristic length, l_{ch}, of the material and contribute to offsetting the size effect of larger structural members. The effectiveness of fiber usage in beams with various span/depth ratios and the resulting flexural and shear beam design considerations and optimizations will be discussed in future publications.

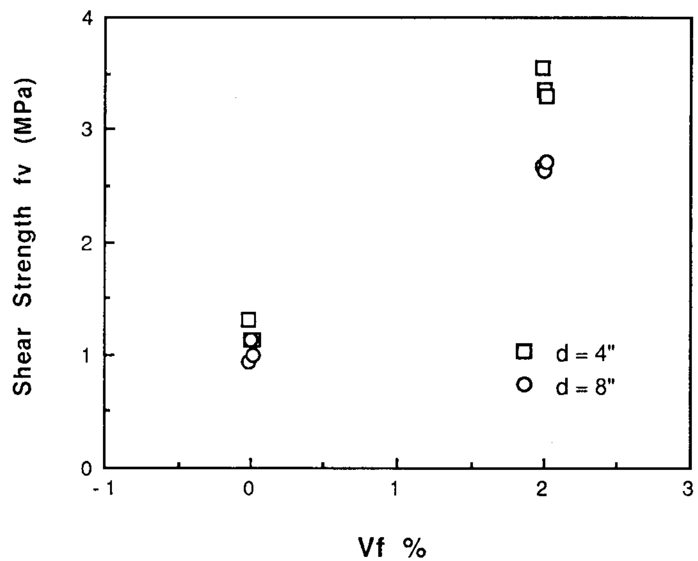

Fig. AD2--Shear strength improvement with 2 percent volume fraction of Kevlar 49 fibers in beams with span/depth ratio of 3

Fracture Toughness of Polymer Concrete

by C. Vipulanandan and N. Dharmarajan

Synopsis: Fracture behavior of epoxy and polyester polymer concrete (PC) systems are investigated in mode I fracture using single edge notched beams with varying notch depths. The beams were loaded in four-point bending . Influence of polymer content on the fracture behavior of epoxy PC and polyester PC at room temperature was studied using uniform Ottawa 20-30 sand. The polymer content was varied between 10% and 18% of the total weight of the composite. The flexural strength of the polymer concrete systems increase with increase in polymer content while the flexural modulus goes through a maximum. The critical stress intensity factor (K_{IC}) was determined by two methods including a method based on crack mouth opening displacement. At the same polymer content, the epoxy PC has a higher fracture toughness than polyester PC. The K_{IC} for epoxy PC and polyester PC increases with increase in polymer content and PC flexural strength.The critical stress intensity factor of PC is represented in terms of polymer content and polymer strength. Numerical tests based on random sampling and stratified sampling procedures were performed to substantiate the experimentally observed fracture toughness values of polymer concrete.

Keywords: cracking (fracturing); epoxy resins; flexural strength; fracture properties; notch sensitivity; polyester resins; polymer concrete; stresses; tests